A WIMF Scheme for the Drift-Flux Two-Phase Flow Model

Steinar Evje[A,B,D], Tore Flåtten[B,A] and Svend Tollak Munkejord[C]

[A]Centre of Mathematics for Applications (CMA),
1053 Blindern, NO-0316 Oslo, Norway
[B]International Research Institute of Stavanger (IRIS),
Prof. Olav Hanssensvei 15, NO-4068 Stavanger, Norway
[C]SINTEF Energy Research, Sem Sælands vei 11, NO-7465 Trondheim, Norway
[D]Corresponding author

Abstract

Two main approaches exist for numerical computation of multiphase flow models. The implicit methods are efficient, yet inaccurate. Better accuracy is achieved by the explicit methods, which on the other hand are time-consuming.

In this paper we investigate generalizations of a class of *hybrid explicit-implicit* numerical schemes [SIAM J. Sci. Comput., 26 (2005), pp. 1449–1484], originally proposed for a two-fluid two-phase flow model. We here outline a framework for extending this class of schemes, denoted as WIMF (weakly implicit mixture flux), to other systems of conservation laws. We apply the strategy to a different two-phase flow model, the *drift-flux* model suitable for describing bubbly two-phase mixtures. Our analysis is based on a simplified formulation of the model, structurally similar to the Euler equations. The main underlying building block is a pressure-based implicit central scheme. Explicit upwind fluxes are incorporated, in a manner ensuring that upwind-type resolution is recovered for a simple contact discontinuity.

The derived scheme is then applied to the general drift-flux model. Numerical simulations demonstrate accuracy, efficiency and a satisfactory level of robustness. Particularly, it is demonstrated that the scheme outperforms an explicit Roe scheme in terms of efficiency and accuracy on slow mass-transport dynamics.

Subject classification

76T10, 76M12, 65M12, 35L65

Key words

two-phase flow, drift-flux model, implicit scheme, contact discontinuity

1 Introduction

Numerical methods for hyperbolic conservation laws may be divided into two main classes; the explicit and the implicit methods. For each wave velocity λ_i associated with the system, the stability of explicit numerical schemes is subject to the CFL criterion

$$\frac{\Delta x}{\Delta t} \geq |\lambda_i|, \tag{1}$$

whereas suitably chosen implicit numerical schemes are unconditionally stable with respect to the time step. However, this improved robustness comes at the price of impaired accuracy.

Consequently, when there is a large disparity between the various eigenvalues λ_i, a possible technique is to split the system into its full wave decomposition and then

- resolve the fast waves by an *implicit* method;
- resolve the slow waves by an *explicit* method.

By this, one aims to obtain an accurate resolution of the slow waves without being hampered by stability requirements pertaining to the fastest waves.

Such *hybrid explicit-implicit* methods are most naturally obtained in the context of *approximate Riemann solvers*; see for instance [7] or [15, 24] for applications to two-phase flows.

However, this full wave structure decomposition is generally computationally costly; in particular, this is the case for standard two-phase flow models [6, 31]. Efficiency considerations motivated us to consider alternative strategies for numerically identifying the various waves of the two-phase system. In a series of papers [10, 11, 12], we investigated a *flux hybridization* technique, where upwind resolution was incorporated into a central pressure-based scheme by a splitting of the convective fluxes into two components.

In [10, 11, 12], we considered the two-fluid two-phase flow model. The primary aim of this paper is to extend the WIMF scheme of [11, 12] to the related *drift-flux* two-phase flow model, allowing us to violate the CFL criterion pertaining to the sonic waves while recovering an explicit upwind resolution of a certain class of material waves. This allows for improved efficiency as well as accuracy compared to fully explicit methods.

Furthermore, we discuss in more detail how appropriate flux hybridizations may be obtained from an analysis of known linear phenomena associated with more general models. In this respect, we aim to shed some light on how the WIMF approach may be extended to other systems of conservation laws.

Our paper is organized as follows: In Section 2, we present the drift-flux model we will be working with. In Section 3, we construct an implicit central scheme for the drift-flux model, based on ideas developed in [11, 12, 14]. In particular, we propose a linearized scheme able to preserve a uniform pressure and velocity field.

In Section 4, we outline a framework for a general construction of WIMF-type schemes. In Section 5, we apply this framework to hybridize the implicit central scheme with an explicit upwind scheme – in such a way that the upwind flux is precisely recovered for a special class of moving or stationary contact discontinuities, while allowing for violation of the sonic CFL criterion. In particular, the resulting WIMF scheme preserves such contacts when the CFL number is optimally chosen.

In Section 6, we present numerical simulations where we compare the behaviour of the WIMF scheme to a fully explicit approximate Riemann solver. The results of the paper are summarized in Section 7.

2 The Two-Phase Flow Model

To avoid excessive computational complexity, workable models describing two-phase flows in pipe networks are conventionally obtained by means of some averaging procedure. Different choices of simplifying assumptions lead to different formulations of such models [30, 32].

The models may be divided in two main classes:

- *two-fluid* models, where equations are written for mass, momentum and energy balances for each fluid separately.
- *mixture* models, where equations for the conservation of physical properties are written for the two-phase mixture.

Mixture models have a reduced number of balance equations compared to two-fluid models, and may be considered as simplifications in terms of mathematical complexity. The missing information must be supplied in terms of additional *closure laws*, often expressed in terms of empirical relations. A more detailed study of the relation between two concrete two-phase models, one two-fluid model and one mixture model, can be found in [13].

When the motions of the two phases are strongly coupled, it would seem that mixture models present several advantages [5]. *Mathematical* difficulties related to non-conservative terms and loss of hyperbolicity, commonly associated with two-fluid models, may be avoided. Some *physical effects*, such as sonic propagation, may be more correctly modelled [16]. Finally, the simplified formulation of the mixture models may allow for more *efficient* computations for industrial applications [25].

For these reasons, mixture models are of significant interest both to the petroleum and nuclear power industries [35]. The particular model investigated in this paper is termed the *drift-flux* model – it is in widespread use by the petroleum industry for modelling the dynamics of oil and gas transport in long production pipelines [24, 25, 28].

2.1 Model Formulation

Following [8], we express the model in the form below:

- Conservation of mass

$$\frac{\partial}{\partial t}\left(\rho_{\mathrm{g}}\alpha_{\mathrm{g}}\right)+\frac{\partial}{\partial x}\left(\rho_{\mathrm{g}}\alpha_{\mathrm{g}}v_{\mathrm{g}}\right)=0, \tag{2}$$

$$\frac{\partial}{\partial t}\left(\rho_{\ell}\alpha_{\ell}\right)+\frac{\partial}{\partial x}\left(\rho_{\ell}\alpha_{\ell}v_{\ell}\right)=0, \tag{3}$$

- Conservation of mixture momentum

$$\frac{\partial}{\partial t}\left(\rho_{\mathrm{g}}\alpha_{\mathrm{g}}v_{\mathrm{g}}+\rho_{\ell}\alpha_{\ell}v_{\ell}\right)+\frac{\partial}{\partial x}\left(\rho_{\mathrm{g}}\alpha_{\mathrm{g}}v_{\mathrm{g}}^{2}+\rho_{\ell}\alpha_{\ell}v_{\ell}^{2}+p\right)=Q, \tag{4}$$

where for phase k the nomenclature is as follows:

ρ_k	-	density,
v_k	-	velocity,
α_k	-	volume fraction,
p	-	pressure common to both phases,
Q	-	non-differential momentum sources (due to gravity, friction, etc.).

The volume fractions satisfy

$$\alpha_{\mathrm{g}}+\alpha_{\ell}=1. \tag{5}$$

Dynamic energy transfers are neglected; we consider isentropic or isothermal flows. In particular, this means that the pressure may be obtained as

$$p=p_{\mathrm{g}}(\rho_{\mathrm{g}})=p_{\ell}(\rho_{\ell}). \tag{6}$$

2.1.1 Thermodynamic Submodels

For the numerical simulations presented in this work we assume that both the gas and liquid phases are compressible, described by the simplified thermodynamic relations

$$\rho_\ell = \rho_{\ell,0} + \frac{p - p_0}{a_\ell^2} \tag{7}$$

and

$$\rho_{\mathrm{g}} = \frac{p}{a_{\mathrm{g}}^2} \tag{8}$$

where

$$p_0 = 1 \text{ bar} = 10^5 \text{ Pa}$$

$$\rho_{\ell,0} = 1000 \text{ kg/m}^3,$$

$$a_{\mathrm{g}}^2 = 10^5 \text{ (m/s)}^2$$

and

$$a_\ell = 10^3 \text{ m/s}.$$

An exception is the numerical example of Section 6.4, where the gas compressibility is altered so that a previously published solution may be reproduced.

2.1.2 Hydrodynamic Submodels

As the model employs a *mixture* momentum equation, additional supplementary relations are required to obtain the information necessary for determining the motion of each phase separately. These constitutive relations, sometimes referred to as the *hydrodynamic closure law* [1], may be expressed in the following general form

$$v_{\mathrm{g}} - v_\ell = \Phi(p, \alpha_\ell, v_{\mathrm{g}}). \tag{9}$$

The relative velocity $v_{\mathrm{r}} = v_{\mathrm{g}} - v_\ell$ between the phases is often referred to as the *slip velocity*; for this reason, the closure law (9) is also commonly known as the *slip relation*.

Of particular interest is the Zuber-Findlay [36] relation

$$v_{\mathrm{g}} = K(\alpha_{\mathrm{g}} v_{\mathrm{g}} + \alpha_\ell v_\ell) + S, \tag{10}$$

where K and S are flow-dependent parameters. This expression is extensively used and is physically relevant for a large class of mixed flow regimes, see for instance [3, 18, 21].

Remark 1. *For industrial cases, Φ is commonly stated as a complex combination of analytic expressions valid for particular flow regimes, experimental correlations, and various switching operators. For practical purposes, it may be considered as a black box. Hence, it is desirable to obtain numerical schemes whose formulation are independent of the particular form of Φ. This aim will be achieved in this paper, although for simplicity, the numerical test cases we investigate will mainly be based on the Zuber-Findlay relation* (10).

3 An Implicit Scheme

In the context of two-phase flows, the implicit schemes currently in use may be divided into two main classes:

- Pressure-based schemes, based on methods originally developed for single-phase gas dynamics [27]. Examples include the OLGA [4] and PeTra [23] computer codes developed for the petroleum industry. These schemes typically require the construction of a staggered grid, and care must be taken to avoid numerical mass leakage.
- Approximate Riemann solvers, for instance the Roe scheme of Toumi [35] or the rough Godunov scheme of Faille and Heintzé [15]. Such schemes are formally conservative and enforce an upwind resolution of all waves; however, they are computationally expensive.

For a nice overview of different numerical schemes from both classes, applied to two-phase models, we refer to the recent book [29]. The approach we take in this work represents an attempt to unify the above two different classes. In particular, we propose in this section a *central pressure-based* scheme of the kind investigated in [14]. Here we follow the standard pressure-based approach of splitting the system into pressure and convection parts, and coupling the pressure calculation to the convective fluxes.

3.1 The Central Pressure-Based Scheme

We consider a spatial grid of N cells, each of size Δx, indexed by

$$j \in [1, \ldots, N]. \tag{11}$$

Furthermore, the time variable is discretized in steps Δt, indexed by the letter n as follows:

$$t^n = t^0 + n\Delta t. \tag{12}$$

Now to adapt the schemes of [11, 12] to the drift-flux model, we divide the calculation into two stages:

1. *Flux linearization:* We formulate linearized evolution equations for the convective mass fluxes, which are solved implicitly coupled to the pressure $p_{j+1/2}^{n+1}$. This is described in Sections 3.1.3–3.1.6.
2. *Conservative update:* Then, in Sections 3.1.7–3.1.8, we describe how to use these fluxes to update the conservative variables while maintaining consistency with the slip relation (9).

3.1.1 Flux Splitting

We write the two-phase flow model (2)–(4) in vector form

$$\frac{\partial \mathbf{U}}{\partial t} + \frac{\partial \mathbf{F}(\mathbf{U})}{\partial x} = \mathbf{Q}(\mathbf{U}), \tag{13}$$

with

$$\mathbf{U} = \begin{bmatrix} \rho_g \alpha_g \\ \rho_\ell \alpha_\ell \\ \rho_g \alpha_g v_g + \rho_\ell \alpha_\ell v_\ell \end{bmatrix}, \quad \mathbf{F}(\mathbf{U}) = \begin{bmatrix} \rho_g \alpha_g v_g \\ \rho_\ell \alpha_\ell v_\ell \\ \rho_g \alpha_g v_g^2 + \rho_\ell \alpha_\ell v_\ell^2 + p \end{bmatrix}, \quad \mathbf{Q}(\mathbf{U}) = \begin{bmatrix} 0 \\ 0 \\ Q \end{bmatrix}. \tag{14}$$

Following [14], we consider a splitting of the flux into convective and pressure parts as follows:

$$\mathbf{F}(\mathbf{U}) = \mathbf{G}(\mathbf{U}) + \mathbf{H}(\mathbf{U}), \tag{15}$$

$$\mathbf{G}(\mathbf{U}) = \begin{bmatrix} \rho_{\mathrm{g}}\alpha_{\mathrm{g}}v_{\mathrm{g}} \\ \rho_\ell\alpha_\ell v_\ell \\ \rho_{\mathrm{g}}\alpha_{\mathrm{g}}v_{\mathrm{g}}^2 + \rho_\ell\alpha_\ell v_\ell^2 \end{bmatrix}, \qquad \mathbf{H}(\mathbf{U}) = \begin{bmatrix} 0 \\ 0 \\ p \end{bmatrix}. \tag{16}$$

3.1.2 Pressure Evolution Equation

The following partial differential equation holds for evolution of the pressure variable:

$$\frac{\partial p}{\partial t} + \kappa\rho_\ell \frac{\partial}{\partial x}\left(\rho_{\mathrm{g}}\alpha_{\mathrm{g}}v_{\mathrm{g}}\right) + \kappa\rho_{\mathrm{g}}\frac{\partial}{\partial x}\left(\rho_\ell\alpha_\ell v_\ell\right) = 0, \tag{17}$$

where

$$\kappa = \frac{1}{\left(\partial\rho_{\mathrm{g}}/\partial p\right)\rho_\ell\alpha_{\mathrm{g}} + \left(\partial\rho_\ell/\partial p\right)\rho_{\mathrm{g}}\alpha_\ell}. \tag{18}$$

The derivation is based on the mass equations (2)–(3), and is detailed in [10, 11]. In Section 3.1.3–3.1.5 we mainly deal with the numerical flux associated with the **G** component, whereas the numerical flux associated with **H** is treated in Section 3.1.6.

3.1.3 Convective Flux Linearization

A flux-conservative discretization of the mass equations (2) and (3) reads

$$\frac{(\rho_k\alpha_k)_j^{n+1} - (\rho_k\alpha_k)_j^n}{\Delta t} + \frac{(\widetilde{\rho_k\alpha_k v_k})_{j+1/2} - (\widetilde{\rho_k\alpha_k v_k})_{j-1/2}}{\Delta x} = 0, \tag{19}$$

where $k \in \mathrm{g}, \ell$. In [14], we argued that the *modified Lax-Friedrichs fluxes*

$$(\widetilde{\rho_k\alpha_k v_k})_{j+1/2} = \frac{1}{2}\left((\rho_k\alpha_k v_k)_j^{n+1} + (\rho_k\alpha_k v_k)_{j+1}^{n+1}\right) + \frac{1}{4}\frac{\Delta x}{\Delta t}\left((\rho_k\alpha_k)_j^n - (\rho_k\alpha_k)_{j+1}^n\right), \tag{20}$$

with an *implicit* central flux approximation and an *explicit* numerical viscosity, naturally lead to a numerically well-behaved pressure-momentum coupling. For the two-fluid model, the momentum variables are solved separately, so (20) directly gives rise to a linearly implicit scheme as described in [11, 12].

However, for the drift-flux model, the individual momentum variables are generally connected through a nonlinear slip relation. Consequently, a scheme based directly on the fluxes (20) may require an iterative solution procedure. This is undesirable.

Hence we propose to replace the expression (20) with a *linearly implicit* approximation:

$$(\widetilde{\rho_k\alpha_k v_k})_{j+1/2} = \frac{1}{2}\left((\widetilde{\rho_k\alpha_k v_k})_j + (\widetilde{\rho_k\alpha_k v_k})_{j+1}\right) + \frac{1}{4}\frac{\Delta x}{\Delta t}\left((\rho_k\alpha_k)_j^n - (\rho_k\alpha_k)_{j+1}^n\right), \tag{21}$$

where the linearization

$$(\widetilde{\rho_k\alpha_k v_k})_j = (\rho_k\alpha_k v_k)_j^n + \mathcal{O}(\Delta t) \approx (\rho_k\alpha_k v_k)_j^{n+1} \tag{22}$$

will be defined in the following.

3.1.4 Convection Evolution Equations

We seek a linearization (21) satisfying the following requirements:

R1: The linearization should be independent of the particular choice of slip relation Φ;

R2: The linearization should preserve a uniform velocity and pressure field.

These considerations suggest that we should base the linearization on the slip relation $\Phi = 0$, equivalently expressed as $v = v_{\mathrm{g}} = v_\ell$. If we linearize around this condition, the following evolution equations hold for the momentum variables:

$$\frac{\partial}{\partial t}\left(\rho_{\mathrm{g}}\alpha_{\mathrm{g}}v_{\mathrm{g}}\right) + \frac{\partial}{\partial x}\left(\rho_{\mathrm{g}}\alpha_{\mathrm{g}}v_{\mathrm{g}}^2\right) + \frac{m_{\mathrm{g}}}{\rho}\frac{\partial p}{\partial x} = \frac{m_{\mathrm{g}}}{\rho}Q + \mathcal{O}(\Phi) \tag{23}$$

and

$$\frac{\partial}{\partial t}\left(\rho_\ell\alpha_\ell v_\ell\right) + \frac{\partial}{\partial x}\left(\rho_\ell\alpha_\ell v_\ell^2\right) + \frac{m_\ell}{\rho}\frac{\partial p}{\partial x} = \frac{m_\ell}{\rho}Q + \mathcal{O}(\Phi), \tag{24}$$

where we have used the shorthands

$$m_k = \rho_k\alpha_k, \qquad \rho = \rho_{\mathrm{g}}\alpha_{\mathrm{g}} + \rho_\ell\alpha_\ell. \tag{25}$$

A derivation of these equations may be found in [13]. In the following, we will use precisely (23) and (24) as the basis to obtain the approximation (22).

3.1.5 Convective Flux Evaluation

We discretize (23) and (24) as

$$\begin{aligned}\frac{(\widetilde{\rho_{\mathrm{g}}\alpha_{\mathrm{g}}v_{\mathrm{g}}})_j - (\rho_{\mathrm{g}}\alpha_{\mathrm{g}}v_{\mathrm{g}})_j^n}{\Delta t} &+ \frac{\left(\widetilde{\rho_{\mathrm{g}}\alpha_{\mathrm{g}}v_{\mathrm{g}}^2}\right)_{j+1/2} - \left(\widetilde{\rho_{\mathrm{g}}\alpha_{\mathrm{g}}v_{\mathrm{g}}^2}\right)_{j-1/2}}{\Delta x} \\ &+ \left(\frac{m_{\mathrm{g}}}{\rho}\right)_j^n \frac{p_{j+1/2}^{n+1} - p_{j-1/2}^{n+1}}{\Delta x} = \left(\widetilde{\frac{m_{\mathrm{g}}}{\rho}Q}\right)_j\end{aligned} \tag{26}$$

and

$$\begin{aligned}\frac{(\widetilde{\rho_\ell\alpha_\ell v_\ell})_j - (\rho_\ell\alpha_\ell v_\ell)_j^n}{\Delta t} &+ \frac{\left(\widetilde{\rho_\ell\alpha_\ell v_\ell^2}\right)_{j+1/2} - \left(\widetilde{\rho_\ell\alpha_\ell v_\ell^2}\right)_{j-1/2}}{\Delta x} \\ &+ \left(\frac{m_\ell}{\rho}\right)_j^n \frac{p_{j+1/2}^{n+1} - p_{j-1/2}^{n+1}}{\Delta x} = \left(\widetilde{\frac{m_\ell}{\rho}Q}\right)_j.\end{aligned} \tag{27}$$

That is, the mass flux $(\widetilde{\rho_k\alpha_k v_k})_{j+1/2}$ is defined by (21), (26), and (27). Here we must specify the fluxes $p_{j+1/2}^{n+1}$ and $\left(\widetilde{\rho_k\alpha_k v_k^2}\right)_{j+1/2}$, and we start with the latter. The pressure flux is specified in Section 3.1.6 since it also directly appears in the $\mathbf{H}$ component given in (16). Following [14], we use linearized modified Lax-Friedrichs fluxes also for momentum convection, consistent with (21), giving

$$(\widetilde{\rho_{\mathrm{g}}\alpha_{\mathrm{g}}v_{\mathrm{g}}^2})_{j+1/2} = \frac{1}{2}(v_{\mathrm{g}}^n \cdot \widetilde{\rho_{\mathrm{g}}\alpha_{\mathrm{g}}v_{\mathrm{g}}})_j + \frac{1}{2}(v_{\mathrm{g}}^n \cdot \widetilde{\rho_{\mathrm{g}}\alpha_{\mathrm{g}}v_{\mathrm{g}}})_{j+1} + \frac{1}{4}\frac{\Delta x}{\Delta t}\left((\rho_{\mathrm{g}}\alpha_{\mathrm{g}}v_{\mathrm{g}})_j^n - (\rho_{\mathrm{g}}\alpha_{\mathrm{g}}v_{\mathrm{g}})_{j+1}^n\right) \tag{28}$$

and

$$\widetilde{(\rho_\ell\alpha_\ell v_\ell^2)}_{j+1/2} = \frac{1}{2}(v_\ell^n \cdot \widetilde{\rho_\ell\alpha_\ell v_\ell})_j + \frac{1}{2}(v_\ell^n \cdot \widetilde{\rho_\ell\alpha_\ell v_\ell})_{j+1} + \frac{1}{4}\frac{\Delta x}{\Delta t}\left((\rho_\ell\alpha_\ell v_\ell)_j^n - (\rho_\ell\alpha_\ell v_\ell)_{j+1}^n\right). \quad (29)$$

By this linearization, the numerical flux associated with the full convective flux vector $\mathbf{G}$ in (16) is the following one

$$\tilde{\mathbf{G}}_{j+1/2} = \begin{bmatrix} \widetilde{(\rho_g\alpha_g v_g)}_{j+1/2} \\ \widetilde{(\rho_\ell\alpha_\ell v_\ell)}_{j+1/2} \\ \widetilde{(\rho_g\alpha_g v_g^2)}_{j+1/2} + \widetilde{(\rho_\ell\alpha_\ell v_\ell^2)}_{j+1/2} \end{bmatrix}. \quad (30)$$

3.1.6 The Pressure Flux

The pressure flux $p_{j+1/2}^{n+1}$ is obtained through the following discretization of the pressure equation (17):

$$\frac{p_{j+1/2}^{n+1} - \frac{1}{2}(p_j^n + p_{j+1}^n)}{\Delta t} + [\kappa\rho_\ell]\frac{\widetilde{(\rho_g\alpha_g v_g)}_{j+1} - \widetilde{(\rho_g\alpha_g v_g)}_j}{\Delta x} + \left[\kappa\rho_g\right]\frac{\widetilde{(\rho_\ell\alpha_\ell v_\ell)}_{j+1} - \widetilde{(\rho_\ell\alpha_\ell v_\ell)}_j}{\Delta x} = 0. \quad (31)$$

Note that the equations (26) and (27) (together with (28) and (29)) are solved implicitly coupled with the discretization (31). These equations constitute a linear system $\mathbf{Ax} = \mathbf{b}$, where $\mathbf{A}$ is a banded matrix with two subdiagonals and two superdiagonals. This is fully analogous to the pressure-momentum coupling used in [11, 12].

Following [10, 12], the coefficient variables $[\cdot] = (\cdot)_{j+1/2}^n$ are obtained from the following relations:

$$\alpha_{k,j+1/2} = \frac{1}{2}(\alpha_{k,j} + \alpha_{k,j+1}), \quad (32)$$

$$\rho_{k,j+1/2} = \frac{1}{2}(\rho_{k,j} + \rho_{k,j+1}) \quad (33)$$

for phase k.

3.1.7 Conservative Update

Having obtained the flux component $\tilde{\mathbf{G}}_{j+1/2}$, as given by (30), as well as

$$\mathbf{H}_{j+1/2} = \begin{bmatrix} 0 \\ 0 \\ p_{j+1/2}^{n+1} \end{bmatrix} \quad (34)$$

through the implicit couplings (26), (27) and (31), we may formulate a conservative scheme as follows:

$$\frac{\mathbf{U}_j^{n+1} - \mathbf{U}_j^n}{\Delta t} + \frac{\mathbf{F}_{j+1/2} - \mathbf{F}_{j-1/2}}{\Delta x} = \mathbf{Q}_j, \quad (35)$$

where

$$\mathbf{F}_{j+1/2} = \tilde{\mathbf{G}}_{j+1/2} + \mathbf{H}_{j+1/2}. \quad (36)$$

Hence we have formulated a *fully conservative*, *linearly implicit* scheme.

3.1.8 Physical Variables

From the components $(U_1, U_2, U_3)_j^{n+1}$ of the conservative variables $\mathbf{U}_j^{n+1}$, we may obtain physical variables $(p, \alpha_\ell, v_g, v_\ell)_j^{n+1}$ as follows:

- *Mass variables*. We may write $\alpha_g + \alpha_\ell = 1$ as
$$\frac{U_1}{\rho_g(p)} + \frac{U_2}{\rho_\ell(p)} = 1, \tag{37}$$
which may be solved for p and consequently α_ℓ.

- *Velocities*. The velocities v_g and v_ℓ are obtained from simultaneously solving the equations
$$U_3 = U_1 v_g + U_2 v_\ell \tag{38}$$
$$v_g - v_\ell = \Phi(p, \alpha_\ell, v_g). \tag{39}$$

As noted in [14], our central pressure-based schemes are strongly related to the FORCE scheme studied by Toro [34], and fall into a class we denoted as X-FORCE (eXtended FORCE) schemes [14]. This motivates the following terminology:

Definition 1. *The numerical scheme described in Section 3.1, applied to the drift-flux model described in Section 2, will for the purposes of this paper be denoted as the* **p-XF** *(pressure-based X-FORCE) scheme.*

4 The WIMF Scheme

The p-XF scheme derived above evolves both the convective and pressure fluxes in an implicit manner, and hence is potentially stable under violation of the CFL criterion (1) for the various wave speeds λ_i.

On the other hand, the scheme reduces to an *implicit modified Lax-Friedrichs scheme* for linear advection. The goal of this section is to hybridize the p-XF scheme with an explicit advection upwind scheme, such that the hybrid scheme provides:

- An implicit central approximation of *pressure* waves, allowing for a stable resolution of such waves under violation of the sonic CFL criterion.

- An explicit upwind approximation of *material* waves, allowing for more accurate resolution of such waves.

To this end, we follow the WIMF strategy introduced in [11]. Using this approach, we avoid a full decomposition of the system into sonic and material waves. Rather, a key idea behind the WIMF approach is that an *approximate* wave splitting, based on simple linear solutions inherent in the model, may be sufficient for practical computations.

In the following, we first discuss how we may go about extending the WIMF scheme of [11, 12] to more general conservation laws. In Section 5, we then present a particular WIMF scheme adapted to the general drift-flux model. Here we obtain an approximate wave splitting by analysing linear phenomena associated with the $\Phi = 0$ model, and apply this splitting to the general case of arbitrary Φ.

4.1 A General Framework

We consider the system of conservation laws

$$\frac{\partial \mathbf{U}}{\partial t} + \frac{\partial \mathbf{F}(\mathbf{U})}{\partial x} = 0, \tag{40}$$

where $\mathbf{U}$ is an N-vector.

We now assume that the vector of conserved variables can be expressed in terms of reduced variables $\boldsymbol{\mu}(\mathbf{U})$ and $\boldsymbol{\nu}(\mathbf{U})$, i.e.

$$\mathbf{U} = \mathbf{U}(\boldsymbol{\mu}, \boldsymbol{\nu}), \tag{41}$$

where $\boldsymbol{\mu}$ and $\boldsymbol{\nu}$ are also N-vectors. This may be expressed in differential form as

$$\mathrm{d}\mathbf{U} = \left(\frac{\partial \mathbf{U}}{\partial \boldsymbol{\mu}}\right)_{\boldsymbol{\nu}} \mathrm{d}\boldsymbol{\mu} + \left(\frac{\partial \mathbf{U}}{\partial \boldsymbol{\nu}}\right)_{\boldsymbol{\mu}} \mathrm{d}\boldsymbol{\nu}. \tag{42}$$

We are concerned here with identifying certain aspects of the model that we want to resolve in detail. In the current context, we wish to identify *linear* phenomena associated with the model. Hence we assume that the splitting (42) can, and has been, chosen such that (40) supports a linear wave solution in $\boldsymbol{\mu}$; in particular, we assume that

$$\mathrm{d}\boldsymbol{\nu} \equiv 0 \tag{43}$$

implies

$$\frac{\partial \boldsymbol{\mu}}{\partial t} + \lambda \frac{\partial \boldsymbol{\mu}}{\partial x} = 0 \tag{44}$$

for some constant wave speed $\lambda(\boldsymbol{\nu})$.

Such a linear solution may potentially be recognized from physical considerations; in Section 5 we consider the linear advection resulting from assuming a uniform pressure and velocity field.

4.1.1 Motivation

For an accurate resolution of these linear waves, we would like our hybrid scheme to reduce to the explicit upwind scheme for the particular solution (44). In particular, if (43)–(44) hold, the numerical flux should satisfy

$$\begin{aligned} \tilde{\mathbf{F}}_{j+1/2} &= \mathbf{F}(\mathbf{U}_j^n) \quad \text{for } \lambda > 0, \\ \tilde{\mathbf{F}}_{j+1/2} &= \mathbf{F}(\mathbf{U}_{j+1}^n) \quad \text{for } \lambda < 0. \end{aligned} \tag{45}$$

We now assume that we have at our disposal the following building blocks:

1. Some explicit flux $\tilde{\mathbf{F}}^{\mathrm{U}}$ satisfying (45), but not necessarily stable under CFL violation;
2. Some implicit flux $\tilde{\mathbf{F}}^{\mathrm{I}}$, stable under CFL violation, but not necessarily satisfying (45).

In the following, we will seek an expression for a *hybrid* numerical flux based on the components $\tilde{\mathbf{F}}^{\mathrm{I}}$ and $\tilde{\mathbf{F}}^{\mathrm{U}}$, combining the desirable features of both, for a model where appropriate variables $\boldsymbol{\mu}$ and $\boldsymbol{\nu}$ can be identified.

4.1.2 The Reduced Evolution Equations

We observe that (40) may be manipulated to yield evolution equations for $\boldsymbol{\mu}$ and $\boldsymbol{\nu}$:

$$\frac{\partial \boldsymbol{\mu}}{\partial \mathbf{U}}\left(\frac{\partial \mathbf{U}}{\partial t}+\frac{\partial \mathbf{F}(\mathbf{U})}{\partial x}\right)=\frac{\partial \boldsymbol{\mu}}{\partial t}+\frac{\partial \boldsymbol{\mu}}{\partial \mathbf{U}}\frac{\partial \mathbf{F}(\mathbf{U})}{\partial x} = 0, \tag{46}$$

$$\frac{\partial \boldsymbol{\nu}}{\partial \mathbf{U}}\left(\frac{\partial \mathbf{U}}{\partial t}+\frac{\partial \mathbf{F}(\mathbf{U})}{\partial x}\right)=\frac{\partial \boldsymbol{\nu}}{\partial t}+\frac{\partial \boldsymbol{\nu}}{\partial \mathbf{U}}\frac{\partial \mathbf{F}(\mathbf{U})}{\partial x} = 0. \tag{47}$$

A semi-discrete formulation of (46) and (47) reads:

$$\frac{\mathrm{d}\boldsymbol{\mu}_j}{\mathrm{d}t}+\left[\frac{\partial \boldsymbol{\mu}}{\partial \mathbf{U}}\right]_j\frac{\mathbf{F}^{\boldsymbol{\mu}}_{j+1/2}-\mathbf{F}^{\boldsymbol{\mu}}_{j-1/2}}{\Delta x} = 0, \tag{48}$$

$$\frac{\mathrm{d}\boldsymbol{\nu}_j}{\mathrm{d}t}+\left[\frac{\partial \boldsymbol{\nu}}{\partial \mathbf{U}}\right]_j\frac{\mathbf{F}^{\boldsymbol{\nu}}_{j+1/2}-\mathbf{F}^{\boldsymbol{\nu}}_{j-1/2}}{\Delta x} = 0. \tag{49}$$

As stated in the previous section, it is desirable to use an *upwind flux* to resolve the linear phenomenon associated with $\boldsymbol{\mu}$ and an *implicit flux* for the variables $\boldsymbol{\nu}$ that do not take part in the linear wave. Hence we take:

$$\mathbf{F}^{\boldsymbol{\mu}}_{j+1/2} = \tilde{\mathbf{F}}^{\mathrm{U}}_{j+1/2}, \tag{50}$$

$$\mathbf{F}^{\boldsymbol{\nu}}_{j+1/2} = \tilde{\mathbf{F}}^{\mathrm{I}}_{j+1/2}. \tag{51}$$

4.1.3 A Non-Conservative Method

By integrating over the cell j and taking the time derivative, we can rewrite the definition (42) as

$$\frac{\mathrm{d}\mathbf{U}_j}{\mathrm{d}t}=\left[\left(\frac{\partial \mathbf{U}}{\partial \boldsymbol{\mu}}\right)_{\boldsymbol{\nu}}\right]_j\frac{\mathrm{d}\boldsymbol{\mu}_j}{\mathrm{d}t}+\left[\left(\frac{\partial \mathbf{U}}{\partial \boldsymbol{\nu}}\right)_{\boldsymbol{\mu}}\right]_j\frac{\mathrm{d}\boldsymbol{\nu}_j}{\mathrm{d}t}. \tag{52}$$

By (48)–(51), this can be reformulated as a *non-conservative* semi-discrete scheme for $\mathbf{U}$ directly:

$$\frac{\mathrm{d}\mathbf{U}_j}{\mathrm{d}t}+\left[\left(\frac{\partial \mathbf{U}}{\partial \boldsymbol{\mu}}\right)_{\boldsymbol{\nu}}\frac{\partial \boldsymbol{\mu}}{\partial \mathbf{U}}\right]_j\frac{\tilde{\mathbf{F}}^{\mathrm{U}}_{j+1/2}-\tilde{\mathbf{F}}^{\mathrm{U}}_{j-1/2}}{\Delta x}+\left[\left(\frac{\partial \mathbf{U}}{\partial \boldsymbol{\nu}}\right)_{\boldsymbol{\mu}}\frac{\partial \boldsymbol{\nu}}{\partial \mathbf{U}}\right]_j\frac{\tilde{\mathbf{F}}^{\mathrm{I}}_{j+1/2}-\tilde{\mathbf{F}}^{\mathrm{I}}_{j-1/2}}{\Delta x}=0. \tag{53}$$

This scheme is derived from the motivations stated in Section 4.1.1 and is consequently expected to combine the benefits of an explicit and implicit flux in a desirable manner. However, a major drawback is that the scheme (53) is not in conservation form. This has several negative consequences; the most serious of which being that the scheme will generally not converge to the correct solution in the presence of discontinuities [22]. Hence we *do not* propose to use (53) for practical computations. Rather, we want to use (53) as a guideline for constructing a more appropriate scheme in conservation form, while retaining the properties that formed the motivation for (53).

4.1.4 The WIMF Flux Hybridization

In this section, we modify the scheme (53) so that it can be written in conservation form:

$$\frac{\mathbf{U}^{n+1}_j-\mathbf{U}^n_j}{\Delta t}+\frac{\mathbf{F}_{j+1/2}-\mathbf{F}_{j-1/2}}{\Delta x}=0, \tag{54}$$

with an appropriately chosen numerical flux function $\mathbf{F}_{j+1/2}$.

Our starting point is the observation that (53) *does* take such a form for the special case that the coefficients are constant. More precisely, when

$$\left[\left(\frac{\partial \mathbf{U}}{\partial \boldsymbol{\mu}}\right)_{\boldsymbol{\nu}} \frac{\partial \boldsymbol{\mu}}{\partial \mathbf{U}}\right]_j = \left[\left(\frac{\partial \mathbf{U}}{\partial \boldsymbol{\mu}}\right)_{\boldsymbol{\nu}} \frac{\partial \boldsymbol{\mu}}{\partial \mathbf{U}}\right]_{j+1} = \left(\frac{\partial \mathbf{U}}{\partial \boldsymbol{\mu}}\right)_{\boldsymbol{\nu}} \frac{\partial \boldsymbol{\mu}}{\partial \mathbf{U}} \tag{55}$$

and

$$\left[\left(\frac{\partial \mathbf{U}}{\partial \boldsymbol{\nu}}\right)_{\boldsymbol{\mu}} \frac{\partial \boldsymbol{\nu}}{\partial \mathbf{U}}\right]_j = \left[\left(\frac{\partial \mathbf{U}}{\partial \boldsymbol{\nu}}\right)_{\boldsymbol{\mu}} \frac{\partial \boldsymbol{\nu}}{\partial \mathbf{U}}\right]_{j+1} = \left(\frac{\partial \mathbf{U}}{\partial \boldsymbol{\nu}}\right)_{\boldsymbol{\mu}} \frac{\partial \boldsymbol{\nu}}{\partial \mathbf{U}}, \tag{56}$$

the numerical flux function of (54) can be written as

$$\mathbf{F}_{j+1/2} = \left(\frac{\partial \mathbf{U}}{\partial \boldsymbol{\mu}}\right)_{\boldsymbol{\nu}} \frac{\partial \boldsymbol{\mu}}{\partial \mathbf{U}} \tilde{\mathbf{F}}^{\mathrm{U}}_{j+1/2} + \left(\frac{\partial \mathbf{U}}{\partial \boldsymbol{\nu}}\right)_{\boldsymbol{\mu}} \frac{\partial \boldsymbol{\nu}}{\partial \mathbf{U}} \tilde{\mathbf{F}}^{\mathrm{I}}_{j+1/2}. \tag{57}$$

In light of this, we propose to base the scheme on the following criteria:

C1: The scheme should be in conservation form (54);

C2: The numerical flux $\mathbf{F}_{j+1/2}$ should be a hybridization of $\tilde{\mathbf{F}}^{\mathrm{U}}_{j+1/2}$ and $\tilde{\mathbf{F}}^{\mathrm{I}}_{j+1/2}$;

C3: The hybridization should reduce to (57) whenever $\mathbf{U} = \mathbf{U}_j = \mathbf{U}_{j+1}$.

It is now straightforward to see that these properties are satisfied by the following generalization of (57):

$$\mathbf{F}_{j+1/2} = \left[\left(\frac{\partial \mathbf{U}}{\partial \boldsymbol{\mu}}\right)_{\boldsymbol{\nu}} \frac{\partial \boldsymbol{\mu}}{\partial \mathbf{U}}\right]_{j+1/2} \tilde{\mathbf{F}}^{\mathrm{U}}_{j+1/2} + \left[\left(\frac{\partial \mathbf{U}}{\partial \boldsymbol{\nu}}\right)_{\boldsymbol{\mu}} \frac{\partial \boldsymbol{\nu}}{\partial \mathbf{U}}\right]_{j+1/2} \tilde{\mathbf{F}}^{\mathrm{I}}_{j+1/2}, \tag{58}$$

where the coefficient variables $[\cdot]_{j+1/2}$ are evaluated at some average state $\mathbf{U}_{j+1/2}$.

We may now state the following proposition:

Proposition 1. *The hybrid fluxes $\tilde{\mathbf{F}}_{j+1/2}$ (58) are consistent provided the basic fluxes $\tilde{\mathbf{F}}^{\mathrm{U}}$ and $\tilde{\mathbf{F}}^{\mathrm{I}}$ are consistent; i.e.*

$$\tilde{\mathbf{F}}_{j+1/2}(\mathbf{U}, \ldots, \mathbf{U}) = \mathbf{F}(\mathbf{U}) \tag{59}$$

if

$$\tilde{\mathbf{F}}^{\mathrm{U}}(\mathbf{U}, \ldots, \mathbf{U}) = \mathbf{F}(\mathbf{U}) \quad \textit{and} \quad \tilde{\mathbf{F}}^{\mathrm{I}}(\mathbf{U}, \ldots, \mathbf{U}) = \mathbf{F}(\mathbf{U}). \tag{60}$$

Proof. Substitute

$$\mathrm{d}\boldsymbol{\mu} = \frac{\partial \boldsymbol{\mu}}{\partial \mathbf{U}} \mathrm{d}\mathbf{U} \qquad \text{and} \qquad \mathrm{d}\boldsymbol{\nu} = \frac{\partial \boldsymbol{\nu}}{\partial \mathbf{U}} \mathrm{d}\mathbf{U} \tag{61}$$

in (42), then factor out $\mathrm{d}\mathbf{U}$ to obtain

$$\left(\frac{\partial \mathbf{U}}{\partial \boldsymbol{\mu}}\right)_{\boldsymbol{\nu}} \frac{\partial \boldsymbol{\mu}}{\partial \mathbf{U}} + \left(\frac{\partial \mathbf{U}}{\partial \boldsymbol{\nu}}\right)_{\boldsymbol{\mu}} \frac{\partial \boldsymbol{\nu}}{\partial \mathbf{U}} = \mathbf{I}, \tag{62}$$

and in particular

$$\left[\left(\frac{\partial \mathbf{U}}{\partial \boldsymbol{\mu}}\right)_{\boldsymbol{\nu}} \frac{\partial \boldsymbol{\mu}}{\partial \mathbf{U}}\right]_{j+1/2} + \left[\left(\frac{\partial \mathbf{U}}{\partial \boldsymbol{\nu}}\right)_{\boldsymbol{\mu}} \frac{\partial \boldsymbol{\nu}}{\partial \mathbf{U}}\right]_{j+1/2} = \mathbf{I}, \tag{63}$$

and the result follows from (58). □

Hence (58) is precisely the hybridization of an implicit and explicit flux we propose for constructing a WIMF scheme for a general model equipped with a splitting (42).

5 Application to the Drift-Flux Model

We now derive the specific implementation of the WIMF scheme for the drift-flux two-phase flow model. Using the approach above, we need to identify a variable $\boldsymbol{\mu}$ associated with some linear wave solution of the system. As the wave structure of the system depends upon the slip relation Φ, we will follow the approach used in Section 3.1.4 for the p-XF scheme. That is, we will base our analysis on linearizing the slip relation around $\Phi = 0$, and extend these results to general Φ.

For $\Phi = 0$, there exists a simple connection between the drift-flux model and the Euler model, as noted in [19] and described below.

5.1 Relation to the Euler Model

The drift-flux model (2)–(4) with $v_{\mathrm{g}} = v_\ell = v$ can be written as:

$$\frac{\partial}{\partial t}\left(\rho_{\mathrm{g}}\alpha_{\mathrm{g}}\right) + \frac{\partial}{\partial x}\left(\rho_{\mathrm{g}}\alpha_{\mathrm{g}} v\right) = 0 \tag{64}$$

$$\frac{\partial}{\partial t}\left(\rho_\ell\alpha_\ell\right) + \frac{\partial}{\partial x}\left(\rho_\ell\alpha_\ell v\right) = 0 \tag{65}$$

$$\frac{\partial}{\partial t}(v(\rho_\ell\alpha_\ell + \rho_{\mathrm{g}}\alpha_{\mathrm{g}}) + \frac{\partial}{\partial x}\left(v^2(\rho_\ell\alpha_\ell + \rho_{\mathrm{g}}\alpha_{\mathrm{g}}) + p\right) = 0. \tag{66}$$

If we now define the mixture density

$$\rho = \rho_{\mathrm{g}}\alpha_{\mathrm{g}} + \rho_\ell\alpha_\ell \tag{67}$$

and the gas mass fraction

$$Y = \frac{\rho_{\mathrm{g}}\alpha_{\mathrm{g}}}{\rho}, \tag{68}$$

the $\Phi = 0$ drift-flux model (64)–(66) can be reformulated as

- Conservation of gas mass
$$\frac{\partial}{\partial t}(\rho Y) + \frac{\partial}{\partial x}(\rho Y v) = 0 \tag{69}$$
- Conservation of total mass
$$\frac{\partial \rho}{\partial t} + \frac{\partial}{\partial x}(\rho v) = 0 \tag{70}$$
- Conservation of momentum
$$\frac{\partial}{\partial t}(\rho v) + \frac{\partial}{\partial x}(\rho v^2 + p) = 0, \tag{71}$$

where

$$p = p(m_{\mathrm{g}}, m_\ell) = p(\rho, Y). \tag{72}$$

We recognize this formulation as structurally identical to the Euler model, if we associate the total mass ρ with the density and the gas mass fraction Y with the entropy. In particular, this means that the model (64)–(66) possesses a linear wave moving with the velocity v, transporting the gas mass fraction Y, analogous to the entropy wave of the Euler model.

Remark 2. *So far, we have shown the existence of a linear wave in the $v_\mathrm{g} = v_\ell$ drift-flux model. This corresponds to $K = 1$, $S = 0$ in the Zuber-Findlay relation* (10)*. However, provided the liquid is incompressible, a more general result holds:*

Proposition 2. *The drift-flux model* (2)–(4)*, augmented with the Zuber-Findlay relation* (10) *where K and S are constants, supports a linear wave solution moving with the velocity v_g, provided the liquid is incompressible. The pressure is not necessarily constant across a contact discontinuity in this wave.*

Proof. The proof of this proposition may be found in [19].

□

5.2 The Flux Hybridization

In this section, we derive the WIMF hybridization (58) for the special case of the $v = v_\mathrm{g} = v_\ell$ drift-flux model. Then, from Section 5.3, we describe how this hybridization scheme may be naturally applied to general slip relations Φ.

Based on the equivalence with the Euler system described in Section 5.1, we may conclude that the splitting (42) with

$$\boldsymbol{\mu} = \begin{bmatrix} Y \\ 0 \\ 0 \end{bmatrix} \quad \text{and} \quad \boldsymbol{\nu} = \begin{bmatrix} 0 \\ p \\ v \end{bmatrix}, \tag{73}$$

satisfies the linear wave criterion described by (43)–(44).

We obtain

$$\frac{\partial \boldsymbol{\mu}}{\partial \mathbf{U}} = \frac{1}{\rho^2}\begin{bmatrix} \rho_\ell\alpha_\ell & -\rho_\mathrm{g}\alpha_\mathrm{g} & 0 \\ 0 & 0 & 0 \\ 0 & 0 & 0 \end{bmatrix} \quad \text{and} \quad \frac{\partial \boldsymbol{\nu}}{\partial \mathbf{U}} = \frac{1}{\rho}\begin{bmatrix} 0 & 0 & 0 \\ \kappa\rho\rho_\ell & \kappa\rho\rho_\mathrm{g} & 0 \\ -v & -v & 1 \end{bmatrix} \tag{74}$$

as well as

$$\left(\frac{\partial \mathbf{U}}{\partial \boldsymbol{\mu}}\right)_{\boldsymbol{\nu}} = \rho^2 \begin{bmatrix} 1/\rho_\ell & 0 & 0 \\ -1/\rho_\mathrm{g} & 0 & 0 \\ v(1/\rho_\ell - 1/\rho_\mathrm{g}) & 0 & 0 \end{bmatrix} \tag{75}$$

and

$$\left(\frac{\partial \mathbf{U}}{\partial \boldsymbol{\nu}}\right)_{\boldsymbol{\mu}} = \frac{1}{\kappa}\begin{bmatrix} 0 & \alpha_\mathrm{g}/\rho_\ell & 0 \\ 0 & \alpha_\ell/\rho_\mathrm{g} & 0 \\ 0 & v\left(\alpha_\mathrm{g}/\rho_\ell + \alpha_\ell/\rho_\mathrm{g}\right) & \kappa\rho \end{bmatrix}. \tag{76}$$

5.2.1 The Matrix Coefficients

By (58), the fluxes of the drift-flux WIMF scheme may now be written as

$$\mathbf{F}_{j+1/2} = \mathbf{A}_{j+1/2}\tilde{\mathbf{F}}^\mathrm{U}_{j+1/2} + \mathbf{B}_{j+1/2}\tilde{\mathbf{F}}^\mathrm{I}_{j+1/2}, \tag{77}$$

where

$$\begin{aligned} \mathbf{A}_{j+1/2} &= \left[\left(\frac{\partial \mathbf{U}}{\partial \boldsymbol{\mu}}\right)_{\boldsymbol{\nu}} \frac{\partial \boldsymbol{\mu}}{\partial \mathbf{U}}\right]_{j+1/2} \\ &= \begin{bmatrix} \alpha_\ell & -\rho_\mathrm{g}\alpha_\mathrm{g}/\rho_\ell & 0 \\ -\rho_\ell\alpha_\ell/\rho_\mathrm{g} & \alpha_\mathrm{g} & 0 \\ \rho_\ell\alpha_\ell v(1/\rho_\ell - 1/\rho_\mathrm{g}) & -\rho_\mathrm{g}\alpha_\mathrm{g} v(1/\rho_\ell - 1/\rho_\mathrm{g}) & 0 \end{bmatrix}^n_{j+1/2} \end{aligned} \tag{78}$$

and

$$
\mathbf{B}_{j+1/2} = \left[\left(\frac{\partial \mathbf{U}}{\partial \boldsymbol{v}} \right)_{\boldsymbol{\mu}} \frac{\partial \boldsymbol{v}}{\partial \mathbf{U}} \right]_{j+1/2}
= \begin{bmatrix} \alpha_{\mathrm{g}} & \rho_{\mathrm{g}}\alpha_{\mathrm{g}}/\rho_{\ell} & 0 \\ \rho_{\ell}\alpha_{\ell}/\rho_{\mathrm{g}} & \alpha_{\ell} & 0 \\ -\rho_{\ell}\alpha_{\ell} v(1/\rho_{\ell} - 1/\rho_{\mathrm{g}}) & \rho_{\mathrm{g}}\alpha_{\mathrm{g}} v(1/\rho_{\ell} - 1/\rho_{\mathrm{g}}) & 1 \end{bmatrix}_{j+1/2}^{n}. \tag{79}
$$

To evaluate the coefficient matrices **A** and **B** at cell interfaces, we follow the approach of [10, 12] and define

$$
\alpha_{k,j+1/2} = \frac{1}{2}\left(\alpha_{k,j} + \alpha_{k,j+1}\right) \tag{80}
$$

$$
\rho_{k,j+1/2} = \frac{1}{2}\left(\rho_{k,j} + \rho_{k,j+1}\right)
$$

$$
v_{k,j+1/2} = \frac{1}{2}\left(v_{k,j} + v_{k,j+1}\right) \tag{81}
$$

for phase $k \in \{\mathrm{g}, \ell\}$.

5.2.2 Flux Splitting

We now write

$$
\tilde{\mathbf{F}}^{\mathrm{U}} = \tilde{\mathbf{G}}^{\mathrm{U}} + \tilde{\mathbf{H}}^{\mathrm{U}} \qquad \text{and} \qquad \tilde{\mathbf{F}}^{\mathrm{I}} = \tilde{\mathbf{G}}^{\mathrm{I}} + \tilde{\mathbf{H}}^{\mathrm{I}}, \tag{82}
$$

that is, we split the numerical fluxes into convective and pressure parts as we did in Section 3.1.1, so that (58) can be written as

$$
\tilde{\mathbf{G}}_{j+1/2} = \left[\left(\frac{\partial \mathbf{U}}{\partial \boldsymbol{\mu}} \right)_{\boldsymbol{v}} \frac{\partial \boldsymbol{\mu}}{\partial \mathbf{U}} \right]_{j+1/2} \tilde{\mathbf{G}}^{\mathrm{U}} + \left[\left(\frac{\partial \mathbf{U}}{\partial \boldsymbol{v}} \right)_{\boldsymbol{\mu}} \frac{\partial \boldsymbol{v}}{\partial \mathbf{U}} \right]_{j+1/2} \tilde{\mathbf{G}}^{\mathrm{I}} \tag{83}
$$

and

$$
\tilde{\mathbf{H}}_{j+1/2} = \left[\left(\frac{\partial \mathbf{U}}{\partial \boldsymbol{\mu}} \right)_{\boldsymbol{v}} \frac{\partial \boldsymbol{\mu}}{\partial \mathbf{U}} \right]_{j+1/2} \tilde{\mathbf{H}}^{\mathrm{U}} + \left[\left(\frac{\partial \mathbf{U}}{\partial \boldsymbol{v}} \right)_{\boldsymbol{\mu}} \frac{\partial \boldsymbol{v}}{\partial \mathbf{U}} \right]_{j+1/2} \tilde{\mathbf{H}}^{\mathrm{I}}. \tag{84}
$$

5.2.3 The Hybrid Convective Flux

For the convective upwind fluxes $\tilde{\mathbf{G}}^{\mathrm{U}}_{j+1/2}$, we will use the low Mach-number limit of the advection upstream splitting method, which was investigated as the *CVS* scheme in [9] for the current drift-flux model.

Writing $\tilde{\mathbf{G}}^{\mathrm{U}}_{j+1/2}$ as

$$
\tilde{\mathbf{G}}^{\mathrm{U}}_{j+1/2} = \begin{bmatrix} (\rho_{\mathrm{g}}\alpha_{\mathrm{g}} v_{\mathrm{g}})^{\mathrm{U}}_{j+1/2} \\ (\rho_{\ell}\alpha_{\ell} v_{\ell})^{\mathrm{U}}_{j+1/2} \\ (\rho_{\mathrm{g}}\alpha_{\mathrm{g}} v_{\mathrm{g}}^2)^{\mathrm{U}}_{j+1/2} + (\rho_{\ell}\alpha_{\ell} v_{\ell}^2)^{\mathrm{U}}_{j+1/2} \end{bmatrix}, \tag{85}
$$

we first define the *cell interface* velocities

$$
v_{k,j+1/2} = \frac{1}{2}\left(v^n_{k,j} + v^n_{k,j+1}\right), \tag{86}
$$

and then the convective fluxes

$$(\rho_k \alpha_k v_k)^{\mathrm{U}}_{j+1/2} = \begin{cases} v_{k,j+1/2}(\rho_k \alpha_k)^n_j & \text{if } v_{k,j+1/2} > 0, \\ v_{k,j+1/2}(\rho_k \alpha_k)^n_{j+1} & \text{otherwise} \end{cases} \tag{87}$$

$$(\rho_k \alpha_k v_k^2)^{\mathrm{U}}_{j+1/2} = \begin{cases} v_{k,j+1/2}(\rho_k \alpha_k v_k)^n_j & \text{if } v_{k,j+1/2} > 0, \\ v_{k,j+1/2}(\rho_k \alpha_k v_k)^n_{j+1} & \text{otherwise} \end{cases} \tag{88}$$

for phase $k \in \{\mathrm{g}, \ell\}$.

For the convective implicit part $\tilde{\mathbf{G}}^{\mathrm{I}}_{j+1/2}$ we use the p-XF formulation of the fluxes (30) described in Section 3.1.5.

We then obtain hybrid convective fluxes through (83), using (78) and (79). Note that the convective fluxes $\tilde{\mathbf{G}}^{\mathrm{I}}_{j+1/2}$ are now calculated with the coupling (77) to the upwind flux $\tilde{\mathbf{G}}^{\mathrm{U}}_{j+1/2}$, as described in more detail in Section 5.3.1.

5.2.4 The Hybrid Pressure Flux

We write the pressure fluxes as

$$\tilde{\mathbf{H}}^{\mathrm{U}} = \begin{bmatrix} 0 \\ 0 \\ \tilde{p}^{\mathrm{U}} \end{bmatrix} \quad \text{and} \quad \tilde{\mathbf{H}}^{\mathrm{I}} = \begin{bmatrix} 0 \\ 0 \\ \tilde{p}^{\mathrm{I}} \end{bmatrix}. \tag{89}$$

By (78) and (79), we see that the hybrid pressure flux (84) becomes simply

$$\tilde{\mathbf{H}}_{j+1/2} = \tilde{\mathbf{H}}^{\mathrm{I}}_{j+1/2}, \tag{90}$$

where $\tilde{p}^{\mathrm{I}}$ is given by a fully implicit calculation in the form (31).

Hence no definition of upwind pressure fluxes $\tilde{p}^{\mathrm{U}}$ is required, the WIMF flux hybridization only affects the convective fluxes.

5.3 Implementation Details

Before extending the above results to $\Phi \neq 0$, it may be instructive to focus in more detail on how this WIMF scheme is implemented in practice. As for the p-XF scheme, the computation consists of two steps:

1. *Flux linearization:* We calculate numerical fluxes through the implicit pressure-momentum coupling.

2. *Conservative update:* We use these numerical fluxes to update the conservative variables according to (35).

Note that both these steps incorporate the flux hybridizations (83). We will address them in turn.

5.3.1 Implicit Step

As for the p-XF scheme derived in Section 3, the pressure-momentum coupling yields 3 equations for each computational cell to be implicitly solved over the computational domain. However, an added complication arises from the implicit calculation also involving the explicit part of the system, as given by (77). In the following exposition, we will find it convenient to use the symbol

$$\mathcal{M} = \mathcal{M}_{\mathrm{g}} + \mathcal{M}_{\ell} \tag{91}$$

to denote the total convective momentum flux. Herein

$$\mathcal{M}_{\mathrm{g}} = \rho_{\mathrm{g}}\alpha_{\mathrm{g}}v_{\mathrm{g}}^2, \tag{92}$$

$$\mathcal{M}_{\ell} = \rho_{\ell}\alpha_{\ell}v_{\ell}^2. \tag{93}$$

For convenience of notation, we also use the shorthand

$$[v] = v_{j+1/2}. \tag{94}$$

Applying (77)–(79) and the splitting (82), where we use $\tilde{\mathbf{G}}^{\mathrm{U}}_{j+1/2}$, $\tilde{\mathbf{G}}^{\mathrm{I}}_{j+1/2}$, and $\tilde{\mathbf{H}}^{\mathrm{U}}_{j+1/2}$, $\tilde{\mathbf{H}}^{\mathrm{I}}_{j+1/2}$ as described in Section 5.2.3 and 5.2.4, we see that the WIMF mass fluxes $(\rho_k\alpha_k v_k)^{\mathrm{WIMF}}_{j+1/2}$ can be written in the form

$$\begin{aligned}(\rho_{\mathrm{g}}\alpha_{\mathrm{g}}v_{\mathrm{g}})^{\mathrm{WIMF}}_{j+1/2} = {} & [\alpha_\ell]^n_{j+1/2}(\rho_{\mathrm{g}}\alpha_{\mathrm{g}}v_{\mathrm{g}})^{\mathrm{U}}_{j+1/2} - [\alpha_{\mathrm{g}}\rho_{\mathrm{g}}/\rho_\ell]^n_{j+1/2}(\rho_\ell\alpha_\ell v_\ell)^{\mathrm{U}}_{j+1/2} \\ & + [\alpha_{\mathrm{g}}]^n_{j+1/2}(\widetilde{\rho_{\mathrm{g}}\alpha_{\mathrm{g}}v_{\mathrm{g}}})_{j+1/2} + [\alpha_{\mathrm{g}}\rho_{\mathrm{g}}/\rho_\ell]^n_{j+1/2}(\widetilde{\rho_\ell\alpha_\ell v_\ell})_{j+1/2},\end{aligned} \tag{95}$$

$$\begin{aligned}(\rho_\ell\alpha_\ell v_\ell)^{\mathrm{WIMF}}_{j+1/2} = {} & -[\alpha_\ell\rho_\ell/\rho_{\mathrm{g}}]^n_{j+1/2}(\rho_{\mathrm{g}}\alpha_{\mathrm{g}}v_{\mathrm{g}})^{\mathrm{U}}_{j+1/2} + [\alpha_{\mathrm{g}}]^n_{j+1/2}(\rho_\ell\alpha_\ell v_\ell)^{\mathrm{U}}_{j+1/2} \\ & + [\alpha_\ell\rho_\ell/\rho_{\mathrm{g}}]^n_{j+1/2}(\widetilde{\rho_{\mathrm{g}}\alpha_{\mathrm{g}}v_{\mathrm{g}}})_{j+1/2} + [\alpha_\ell]^n_{j+1/2}(\widetilde{\rho_\ell\alpha_\ell v_\ell})_{j+1/2}.\end{aligned} \tag{96}$$

Similarly, we calculate that

$$\begin{aligned}\mathcal{M}^{\mathrm{WIMF}}_{j+1/2} = {} & [\alpha_\ell v(1-\rho_\ell/\rho_{\mathrm{g}})]^n_{j+1/2}\Big((\rho_{\mathrm{g}}\alpha_{\mathrm{g}}v_{\mathrm{g}})^{\mathrm{U}}_{j+1/2} - (\widetilde{\rho_{\mathrm{g}}\alpha_{\mathrm{g}}v_{\mathrm{g}}})_{j+1/2}\Big) + (\widetilde{\rho_{\mathrm{g}}\alpha_{\mathrm{g}}v_{\mathrm{g}}^2})_{j+1/2} \\ & + [\alpha_{\mathrm{g}}v(1-\rho_{\mathrm{g}}/\rho_\ell)]^n_{j+1/2}\Big((\rho_\ell\alpha_\ell v_\ell)^{\mathrm{U}}_{j+1/2} - (\widetilde{\rho_\ell\alpha_\ell v_\ell})_{j+1/2}\Big) + (\widetilde{\rho_\ell\alpha_\ell v_\ell^2})_{j+1/2},\end{aligned} \tag{97}$$

where

$$(\rho_{\mathrm{g}}\alpha_{\mathrm{g}}v_{\mathrm{g}}^2 + \rho_\ell\alpha_\ell v_\ell^2 + p)^{\mathrm{WIMF}}_{j+1/2} = \mathcal{M}^{\mathrm{WIMF}}_{j+1/2} + \tilde{p}^{\mathrm{I}}_{j+1/2}.$$

Comparing the WIMF convective momentum flux (97) to the sum of (95) and (96) we see that $\mathcal{M}^{\mathrm{WIMF}}_{j+1/2}$ now can be written in terms of the WIMF mass fluxes $(\rho_k\alpha_k v_k)^{\mathrm{WIMF}}_{j+1/2}$ as follows:

$$\mathcal{M}^{\mathrm{WIMF}}_{j+1/2} = \widetilde{\mathcal{M}}_{j+1/2} + [v]\left((\rho_{\mathrm{g}}\alpha_{\mathrm{g}}v_{\mathrm{g}})^{\mathrm{WIMF}}_{j+1/2} - (\widetilde{\rho_{\mathrm{g}}\alpha_{\mathrm{g}}v_{\mathrm{g}}})_{j+1/2} + (\rho_\ell\alpha_\ell v_\ell)^{\mathrm{WIMF}}_{j+1/2} - (\widetilde{\rho_\ell\alpha_\ell v_\ell})_{j+1/2}\right), \tag{98}$$

where

$$\widetilde{\mathcal{M}}_{j+1/2} = (\widetilde{\rho_{\mathrm{g}}\alpha_{\mathrm{g}}v_{\mathrm{g}}^2})_{j+1/2} + (\widetilde{\rho_\ell\alpha_\ell v_\ell^2})_{j+1/2}. \tag{99}$$

This suggests a natural splitting of $\mathcal{M}^{\mathrm{WIMF}}_{j+1/2}$ into

$$\mathcal{M}^{\mathrm{WIMF}}_{j+1/2} = \mathcal{M}^{\mathrm{WIMF}}_{\mathrm{g},j+1/2} + \mathcal{M}^{\mathrm{WIMF}}_{\ell,j+1/2}, \tag{100}$$

where

$$\mathcal{M}^{\mathrm{WIMF}}_{\mathrm{g},j+1/2} = \widetilde{\mathcal{M}}_{\mathrm{g},j+1/2} - [v](\widetilde{\rho_{\mathrm{g}}\alpha_{\mathrm{g}}v_{\mathrm{g}}})_{j+1/2} + [v](\rho_{\mathrm{g}}\alpha_{\mathrm{g}}v_{\mathrm{g}})^{\mathrm{WIMF}}_{j+1/2} \tag{101}$$

$$\mathcal{M}^{\mathrm{WIMF}}_{\ell,j+1/2} = \widetilde{\mathcal{M}}_{\ell,j+1/2} - [v](\widetilde{\rho_\ell\alpha_\ell v_\ell})_{j+1/2} + [v](\rho_\ell\alpha_\ell v_\ell)^{\mathrm{WIMF}}_{j+1/2}. \tag{102}$$

As v is not properly defined when $v_{\mathrm{g}} \neq v_\ell$, we propose to use the following natural modification of (101)–(102) for general slip relations:

$$\mathcal{M}^{\mathrm{WIMF}}_{\mathrm{g},j+1/2} = \widetilde{\mathcal{M}}_{\mathrm{g},j+1/2} - [v_{\mathrm{g}}](\widetilde{\rho_{\mathrm{g}}\alpha_{\mathrm{g}}v_{\mathrm{g}}})_{j+1/2} + [v_{\mathrm{g}}](\rho_{\mathrm{g}}\alpha_{\mathrm{g}}v_{\mathrm{g}})^{\mathrm{WIMF}}_{j+1/2} \tag{103}$$

$$\mathcal{M}^{\mathrm{WIMF}}_{\ell,j+1/2} = \widetilde{\mathcal{M}}_{\ell,j+1/2} - [v_\ell](\widetilde{\rho_\ell\alpha_\ell v_\ell})_{j+1/2} + [v_\ell](\rho_\ell\alpha_\ell v_\ell)^{\mathrm{WIMF}}_{j+1/2}. \tag{104}$$

We now want to represent $\widetilde{\rho_{\mathrm{g}}\alpha_{\mathrm{g}}v_{\mathrm{g}}^2}$ in (26) by (103) and $\widetilde{\rho_\ell\alpha_\ell v_\ell^2}$ in (27) by (104). Thus, the implicit pressure-momentum coupling corresponding to (26), (27), and (31), but now with mixture momentum fluxes $\mathcal{M}^{\mathrm{WIMF}}_{k,j+1/2}$, take the following form:

- *Pressure equation:*

$$\frac{p_{j+1/2}^{n+1} - \frac{1}{2}(p_j^n + p_{j+1}^n)}{\Delta t} + [\kappa\rho_\ell]_{j+1/2} \frac{(\widetilde{\rho_g\alpha_g v_g})_{j+1} - (\widetilde{\rho_g\alpha_g v_g})_j}{\Delta x} + \left[\kappa\rho_g\right]_{j+1/2} \frac{(\widetilde{\rho_\ell\alpha_\ell v_\ell})_{j+1} - (\widetilde{\rho_\ell\alpha_\ell v_\ell})_j}{\Delta x} = 0. \tag{105}$$

- *Gas momentum equation:*

$$\begin{aligned}
&\frac{(\widetilde{\rho_g\alpha_g v_g})_j - (\rho_g\alpha_g v_g)_j^n}{\Delta t} + \frac{\left(\widetilde{\rho_g\alpha_g v_g^2}\right)_{j+1/2} - \left(\widetilde{\rho_g\alpha_g v_g^2}\right)_{j-1/2}}{\Delta x} \\
&- \frac{[v_g\alpha_\ell]_{j+1/2}\left(\widetilde{\rho_g\alpha_g v_g}\right)_{j+1/2} - [v_g\alpha_\ell]_{j-1/2}\left(\widetilde{\rho_g\alpha_g v_g}\right)_{j-1/2}}{\Delta x} \\
&+ \frac{[v_g\alpha_g\rho_g/\rho_\ell]_{j+1/2}\left(\widetilde{\rho_\ell\alpha_\ell v_\ell}\right)_{j+1/2} - [v_g\alpha_g\rho_g/\rho_\ell]_{j-1/2}\left(\widetilde{\rho_\ell\alpha_\ell v_\ell}\right)_{j-1/2}}{\Delta x} \\
&+ \frac{[v_g\alpha_\ell]_{j+1/2}\left(\rho_g\alpha_g v_g\right)_{j+1/2}^{\mathrm{U}} - [v_g\alpha_\ell]_{j-1/2}\left(\rho_g\alpha_g v_g\right)_{j-1/2}^{\mathrm{U}}}{\Delta x} \\
&- \frac{[v_g\alpha_g\rho_g/\rho_\ell]_{j+1/2}(\rho_\ell\alpha_\ell v_\ell)_{j+1/2}^{\mathrm{U}} - [v_g\alpha_g\rho_g/\rho_\ell]_{j-1/2}(\rho_\ell\alpha_\ell v_\ell)_{j-1/2}^{\mathrm{U}}}{\Delta x} \\
&+ \left(\frac{m_g}{\rho}\right)_j^n \frac{p_{j+1/2}^{n+1} - p_{j-1/2}^{n+1}}{\Delta x} = \left(\widetilde{\frac{m_g}{\rho}Q}\right)_j.
\end{aligned} \tag{106}$$

- *Liquid momentum equation:*

$$\begin{aligned}
&\frac{(\widetilde{\rho_\ell\alpha_\ell v_\ell})_j - (\rho_\ell\alpha_\ell v_\ell)_j^n}{\Delta t} + \frac{\left(\widetilde{\rho_\ell\alpha_\ell v_\ell^2}\right)_{j+1/2} - \left(\widetilde{\rho_\ell\alpha_\ell v_\ell^2}\right)_{j-1/2}}{\Delta x} \\
&- \frac{[v_\ell\alpha_g]_{j+1/2}\left(\widetilde{\rho_\ell\alpha_\ell v_\ell}\right)_{j+1/2} - [v_\ell\alpha_g]_{j-1/2}\left(\widetilde{\rho_\ell\alpha_\ell v_\ell}\right)_{j-1/2}}{\Delta x} \\
&+ \frac{[v_\ell\alpha_\ell\rho_\ell/\rho_g]_{j+1/2}\left(\widetilde{\rho_g\alpha_g v_g}\right)_{j+1/2} - [v_\ell\alpha_\ell\rho_\ell/\rho_g]_{j-1/2}\left(\widetilde{\rho_g\alpha_g v_g}\right)_{j-1/2}}{\Delta x} \\
&+ \frac{[v_\ell\alpha_g]_{j+1/2}(\rho_\ell\alpha_\ell v_\ell)_{j+1/2}^{\mathrm{U}} - [v_\ell\alpha_g]_{j-1/2}(\rho_\ell\alpha_\ell v_\ell)_{j-1/2}^{\mathrm{U}}}{\Delta x} \\
&- \frac{[v_\ell\alpha_\ell\rho_\ell/\rho_g]_{j+1/2}\left(\rho_g\alpha_g v_g\right)_{j+1/2}^{\mathrm{U}} - [v_\ell\alpha_\ell\rho_\ell/\rho_g]_{j-1/2}\left(\rho_g\alpha_g v_g\right)_{j-1/2}^{\mathrm{U}}}{\Delta x} \\
&+ \left(\frac{m_\ell}{\rho}\right)_j^n \frac{p_{j+1/2}^{n+1} - p_{j-1/2}^{n+1}}{\Delta x} = \left(\widetilde{\frac{m_\ell}{\rho}Q}\right)_j.
\end{aligned} \tag{107}$$

Here the linearized fluxes are given (as before) by (21) and (28)–(29) as:

$$(\widetilde{\rho_k\alpha_k v_k})_{j+1/2} = \frac{1}{2}\left((\widetilde{\rho_k\alpha_k v_k})_j + (\widetilde{\rho_k\alpha_k v_k})_{j+1}\right) + \frac{1}{4}\frac{\Delta x}{\Delta t}\left((\rho_k\alpha_k)_j^n - (\rho_k\alpha_k)_{j+1}^n\right) \tag{108}$$

and

$$(\widetilde{\rho_k\alpha_k v_k^2})_{j+1/2} = \frac{1}{2}(v_k^n \cdot \widetilde{\rho_k\alpha_k v_k})_j + \frac{1}{2}(v_k^n \cdot \widetilde{\rho_k\alpha_k v_k})_{j+1} + \frac{1}{4}\frac{\Delta x}{\Delta t}\left((\rho_k\alpha_k v_k)_j - (\rho_k\alpha_k v_k)_{j+1}\right)^n. \tag{109}$$

In conclusion, we solve (105)–(107) to obtain the variables $p_{j+1/2}^{n+1}$, $(\widetilde{\rho_g \alpha_g v_g})_j$ and $(\widetilde{\rho_\ell \alpha_\ell v_\ell})_j$ to be used in the following. As for the p-XF scheme, this step requires the inversion of a sparse linear system with a bandwidth of five (pentadiagonal linear system) – where the coefficients become slightly more complicated due to the hybridization (77).

5.3.2 Conservative Update

By use of

$$\tilde{\mathbf{G}}_{j+1/2}^{\mathrm{U}} = \begin{bmatrix} (\rho_g \alpha_g v_g)_{j+1/2}^{\mathrm{U}} \\ (\rho_\ell \alpha_\ell v_\ell)_{j+1/2}^{\mathrm{U}} \\ (\rho_g \alpha_g v_g^2)_{j+1/2}^{\mathrm{U}} + (\rho_\ell \alpha_\ell v_\ell^2)_{j+1/2}^{\mathrm{U}} \end{bmatrix}, \tag{110}$$

and

$$\tilde{\mathbf{G}}_{j+1/2}^{\mathrm{I}} = \begin{bmatrix} (\widetilde{\rho_g \alpha_g v_g})_{j+1/2} \\ (\widetilde{\rho_\ell \alpha_\ell v_\ell})_{j+1/2} \\ (\widetilde{\rho_g \alpha_g v_g^2})_{j+1/2} + (\widetilde{\rho_\ell \alpha_\ell v_\ell^2})_{j+1/2} \end{bmatrix}, \qquad \tilde{\mathbf{H}}^{\mathrm{I}} = \begin{bmatrix} 0 \\ 0 \\ p_{j+1/2}^{n+1} \end{bmatrix}, \tag{111}$$

as defined in Section 5.2.3 and 5.2.4 (note that there is no need to specify $\tilde{\mathbf{H}}^{\mathrm{U}}$ as explained in Section 5.2.4), where the required quantities are obtained through the equations (105)–(107), the numerical scheme can be written in the conservative form

$$\frac{\mathbf{U}_j^{n+1} - \mathbf{U}_j^n}{\Delta t} + \frac{\mathbf{F}_{j+1/2} - \mathbf{F}_{j-1/2}}{\Delta x} = \widetilde{\mathbf{Q}}_j, \tag{112}$$

where $\mathbf{F}_{j+1/2}$ is obtained from (77) and (82). Finally, the physical variables are obtained from $\mathbf{U}_j^{n+1}$ by the procedure described in Section 3.1.8.

5.4 Resolution of Contact Wave

We now provide some attractive theoretical results for the special case of $\Phi = 0$. We consider the linear wave arising from the initial conditions

$$\begin{aligned} p_j &= p \quad \forall j \\ Y_j &= Y(j) \quad \forall j \\ (v_g)_j &= (v_\ell)_j = v \quad \forall j. \end{aligned} \tag{113}$$

In particular, $\boldsymbol{v}$ is constant across the computational domain as stated by (43). The pressure gradient now vanishes from the model (2)–(4), and the solution to the initial value problem (113) is that the distribution of Y will propagate with the uniform velocity v. That is, we have

$$\frac{\partial \boldsymbol{\mu}}{\partial t} + v \frac{\partial \boldsymbol{\mu}}{\partial x} = 0, \tag{114}$$

in accordance with (44).

For the corresponding linear wave associated with the two-fluid model, we proved in [11, 12] that the WIMF scheme possessed the following properties:

(i) WIMF reduces to the explicit upwind flux for the linear wave (113);

(ii) WIMF preserves uniformity of the pressure and velocity field for this linear wave;

(iii) WIMF captures the wave *exactly* on uniform meshes if the time step corresponds to a convective CFL number 1, i.e.

$$\frac{\Delta x}{\Delta t} = v. \tag{115}$$

Here (ii) and (iii) are direct consequences of (i).

An equivalent result holds for the current WIMF scheme for the drift-flux model. In particular, we have the following proposition:

Proposition 3. *The WIMF scheme described in Section 5.3, when applied to the linear wave* (113)*, has a solution that satisfies*

$$
\begin{aligned}
p_j^{n+1} &= p \qquad \forall j, n; && (116)\\
v_j^{n+1} &= v \qquad \forall j, n; && (117)\\
\alpha_{k,j}^{n+1} &= \alpha_{k,j}^{n} - v\frac{\Delta t}{\Delta x}\left(\alpha_{k,j}^{n} - \alpha_{k,j-1}^{n}\right) \qquad \forall j, n \qquad \textit{for } v \geq 0; && (118)\\
\alpha_{k,j}^{n+1} &= \alpha_{k,j}^{n} - v\frac{\Delta t}{\Delta x}\left(\alpha_{k,j+1}^{n} - \alpha_{k,j}^{n}\right) \qquad \forall j, n \qquad \textit{for } v < 0. && (119)
\end{aligned}
$$

Herein

$$(\widetilde{\rho_k \alpha_k v_k})_j = \rho_k \alpha_{k,j}^{n+1} v, \tag{120}$$

where

$$\rho_k \equiv \rho_k(p) = \text{const.} \tag{121}$$

Proof. Substitute (116)–(120) into the equations of Section 5.3. Through a rather lengthy calculation, this will reduce the discrete equations of the WIMF scheme to trivial identities.

□

In particular, this means that (i)–(iii) are satisfied also in the current context. In Section 6.1, these results will be illustrated numerically.

6 Numerical Simulations

In this section, we present some selected numerical examples. We first numerically verify Proposition 3 by studying a simple contact discontinuity for the $\Phi = 0$ model. We then investigate how this behaviour carries over to more general cases, by considering a couple of shock tube problems known from the literature. Reference results will be provided by the explicit Roe scheme described by Flåtten and Munkejord [17].

Finally, we investigate the performance of the scheme on a case more representative of industrial problems; a large-scale mass transport problem given a non-linear slip law.

For the simulations, a convective CFL number is defined as follows

$$C = \frac{\Delta t}{\Delta x} \max_{j,n} |(v_g)_j^n|, \tag{122}$$

as this corresponds to the expected velocity of the mass transport wave associated with the Zuber-Findlay slip law (see Proposition 2).

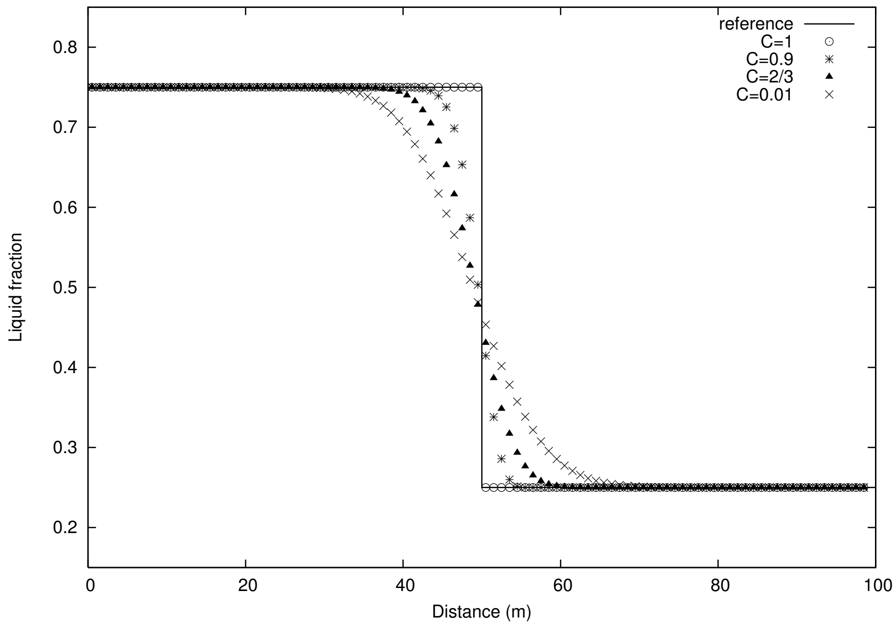

Figure 1: No-slip contact discontinuity, WIMF scheme, 100 cells. Various values of the convective CFL number.

6.1 No-Slip Contact Discontinuity

For our first test, we consider a linear wave where the slip law is given by

$$\Phi = 0. \tag{123}$$

We assume an isolated contact discontinuity separating the states

$$\mathbf{W}_{\mathrm{L}} = \begin{bmatrix} p \\ \alpha_\ell \\ v_{\mathrm{g}} \\ v_\ell \end{bmatrix} = \begin{bmatrix} 10^5 \text{ Pa} \\ 0.75 \\ 10 \text{ m/s} \\ 10 \text{ m/s} \end{bmatrix} \tag{124}$$

and

$$\mathbf{W}_{\mathrm{R}} = \begin{bmatrix} p \\ \alpha_\ell \\ v_{\mathrm{g}} \\ v_\ell \end{bmatrix} = \begin{bmatrix} 10^5 \text{ Pa} \\ 0.25 \\ 10 \text{ m/s} \\ 10 \text{ m/s} \end{bmatrix}. \tag{125}$$

We assume a 100 m long pipe where the discontinuity is initially located at $x = 0$. We use a computational grid of 100 cells and simulate a time of $t = 5.0$ s. The discontinuity will then have moved to the centre of the pipe, being located at $x = 50$ m.

6.1.1 Sensitivity of WIMF to the Convective CFL Number

In Figure 1, the results of WIMF are plotted for various values of the convective CFL number. We observe that WIMF captures the contact exactly for $C = 1$, as stated by Proposition 3. The numerical dissipation increases as C decreases.

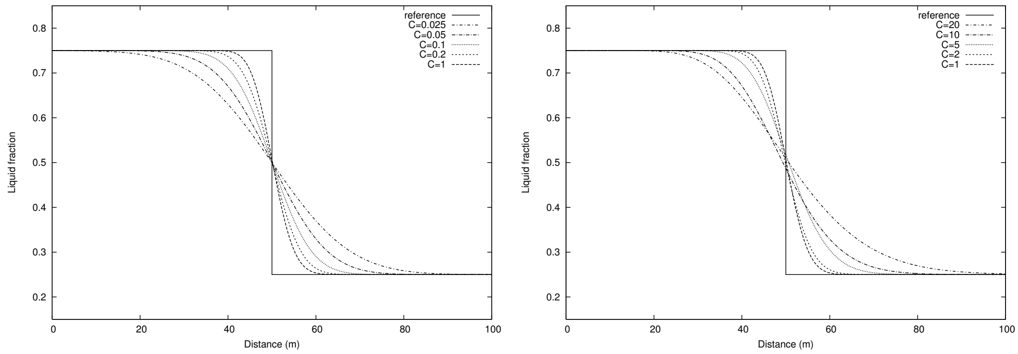

Figure 2: No-slip contact discontinuity, implicit p-XF scheme, 500 cells. Various values of the convective CFL number. Left: Approaching $C = 1$ from below. Right: Approaching $C = 1$ from above.

For $C > 1$, the scheme becomes unstable.

6.1.2 Sensitivity of p-XF to the Convective CFL Number

In Figure 2, the results of p-XF are plotted for various values of the convective CFL number. The scheme obtains maximal accuracy for $C = 1$, and the numerical dissipation increases for both smaller and larger values of C. The dissipation is always larger than for the WIMF scheme, in particular this is the case for $C = 1$. However, the p-XF scheme is observed to be unconditionally stable for this test case.

For both the WIMF and p-XF schemes, we observe that the pressure and velocities remain constant to floating point precision, as is dictated by Proposition 3.

6.2 Dispersed Law Contact Discontinuity

In this section, we consider a more general contact discontinuity where the slip law is given as

$$\Phi = -\delta/\alpha_\ell. \tag{126}$$

This test case is similar to Experiment 4 of Baudin et al. [1].

According to Baudin et al. [1], the slip law (126) describes inclined pipe flows where small gas bubbles are dispersed in the liquid. We follow in their footsteps and use the following value for δ:

$$\delta = 0.045 \text{ m/s}. \tag{127}$$

In the framework of the Zuber-Findlay slip relation (10), the slip relation (126) corresponds to

$$K = 1, \tag{128}$$

$$S = -\delta. \tag{129}$$

The initial states are given by

$$\mathbf{W}_\mathrm{L} = \begin{bmatrix} p \\ \alpha_\ell \\ v_\mathrm{g} \\ v_\ell \end{bmatrix} = \begin{bmatrix} (10^5 + 7.8)\ \text{Pa} \\ 0.9 \\ 1\ \text{m/s} \\ 1.050\ \text{m/s} \end{bmatrix} \tag{130}$$

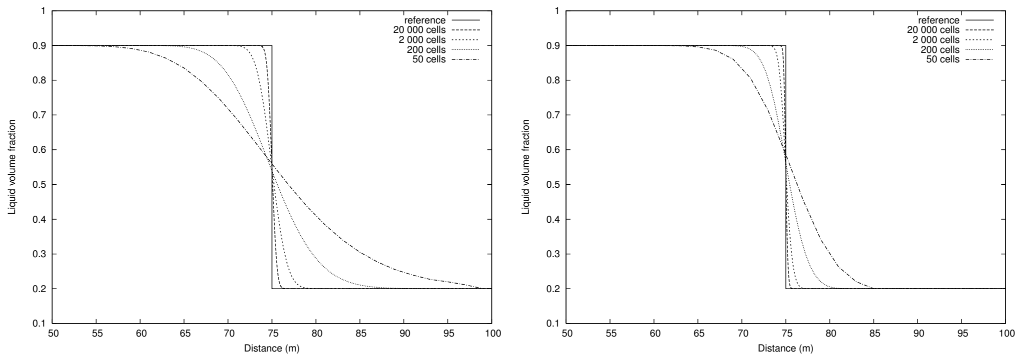

Figure 3: Dispersed law contact discontinuity. Grid refinement for the implicit p-XF and WIMF schemes. Left: p-XF scheme. Right: WIMF scheme.

and

$$\mathbf{W}_{\mathrm{R}} = \begin{bmatrix} p \\ \alpha_\ell \\ v_{\mathrm{g}} \\ v_\ell \end{bmatrix} = \begin{bmatrix} 10^5 \text{ Pa} \\ 0.2 \\ 1 \text{ m/s} \\ 1.224 \text{ m/s} \end{bmatrix}. \tag{131}$$

This discontinuity will now propagate, without change of shape, with the gas velocity $v_{\mathrm{g}} = 1$ m/s, as stated by Proposition 2 (The effect of the liquid compressibility is negligible). We assume a pipe of length 100 m where the contact is initially located at $x = 50$ m. The simulation runs for 25 s.

6.2.1 Convergence Test for p-XF and WIMF

In Figure 3, we investigate the convergence of the WIMF and p-XF schemes as the grid is refined. For the p-XF scheme, we used a convective CFL number $C = 1$, with respect to the gas velocity $v_{\mathrm{g}} = 1$ m/s.

Table 1: Dispersed law contact discontinuity. Convergence rates for the p-XF scheme.

n	cells	$\|\|E\|\|_n$	s_n
1	50	4.818	
2	200	2.405	0.5012
3	2000	0.762	0.4991
4	20000	0.241	0.4999

For the WIMF scheme, where the condition $\Phi = 0$ (under which the flux hybridizations were derived) no longer applies, instabilities occurred for $C > 0.9$. In addition, for $0.75 < C < 0.9$, a persistent overshoot was produced in the contact wave. Hence the WIMF results presented here are produced with a convective CFL number of $C = 0.75$.

However, with this reduction of the CFL number we observe that the WIMF scheme is in fact able to provide an accurate resolution of the contact – the desired upwind-type accuracy is retained, while the sonic CFL criterion is still violated. Convergence rates for the volume fraction variable are given in Tables 1 and 2, where the error is measured in the 1-norm

$$||E|| = \sum_j \Delta x |\alpha_{\mathrm{g},j} - \alpha_{\mathrm{g},j}^{\mathrm{ref}}|, \tag{132}$$

Table 2: Dispersed law contact discontinuity. Convergence rates for the WIMF scheme.

n	cells	$\|\|E\|\|_n$	s_n
1	50	2.260	
2	200	1.094	0.5234
3	2000	0.341	0.5066
4	20000	0.107	0.5014

and the order of convergence s is obtained through

$$s_n = \frac{\ln(||E||_n/||E||_{n-1})}{\ln(\Delta x_n/\Delta x_{n-1})}. \tag{133}$$

Both schemes uniformly approach the expected analytical solution, at similar convergence rates.

6.2.2 Start-up Errors

Due to the particular choice of slip relation, there exists a persistent pressure jump across the contact - whereas the numerical schemes are obtained from considerations of a contact where the pressure is *constant*. As a consequence of this, no result analogous to Proposition 3 holds, and start-up errors in the form of pressure oscillations occur for the first steps of the simulation. We now define the *pressure variation* at each time step as

$$\Delta\tilde{p} = \max_j(p_j^n) - \min_j(p_j^n). \tag{134}$$

With a grid of 20 000 cells and a convective CFL number of $C = 0.75$, a plot of $\Delta\tilde{p}$ against time is given in Figure 4. The behaviour is rather similar for both the p-XF and WIMF schemes, so these oscillations are not primarily associated with the flux hybridization.

This seems to be a price to pay for the simplicity achieved by keeping the schemes independent of the structure of the slip relation Φ. However, we note that the pressure oscillations are rather small and decrease with time, indicating that such start-up errors may be of minor importance for practical calculations. This will be supported by our further numerical examples.

6.3 Zuber-Findlay Shock 1

Using the Zuber-Findlay slip relation with

$$K = 1.07 \tag{135}$$
$$S = 0.216 \text{ m/s}, \tag{136}$$

we consider a shock tube problem also investigated by Evje and Fjelde [8]. The initial states are given by

$$\mathbf{W}_\mathrm{L} = \begin{bmatrix} p \\ \alpha_\ell \\ v_\mathrm{g} \\ v_\ell \end{bmatrix} = \begin{bmatrix} 80450 \text{ Pa} \\ 0.45 \\ 12.659 \text{ m/s} \\ 10.370 \text{ m/s} \end{bmatrix} \tag{137}$$

and

$$\mathbf{W}_\mathrm{R} = \begin{bmatrix} p \\ \alpha_\ell \\ v_\mathrm{g} \\ v_\ell \end{bmatrix} = \begin{bmatrix} 24282 \text{ Pa} \\ 0.45 \\ 1.181 \text{ m/s} \\ 0.561 \text{ m/s} \end{bmatrix}. \tag{138}$$

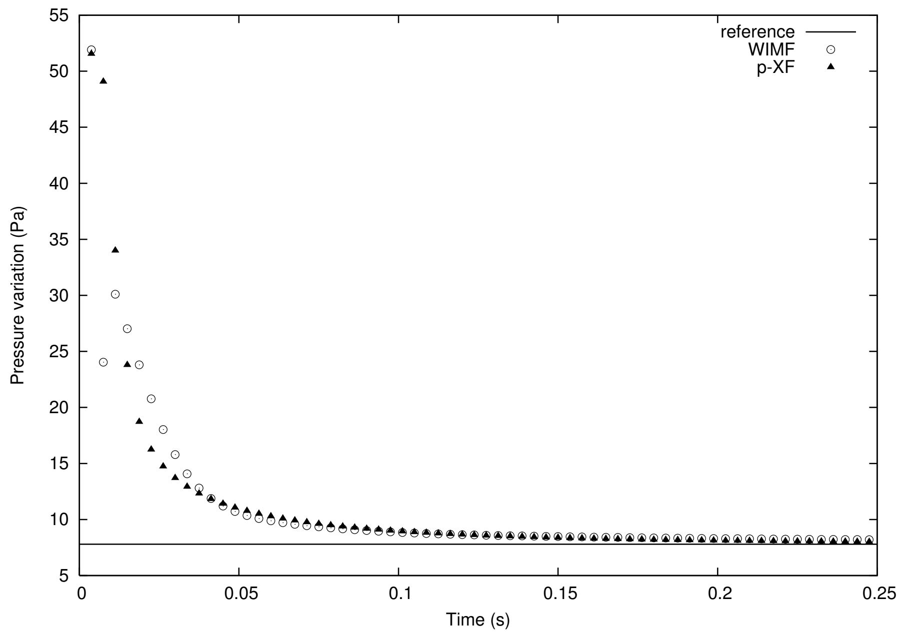

Figure 4: Dispersed law contact discontinuity, start-up errors. Initial pressure oscillations produced by WIMF and p-XF schemes.

The initial discontinuity is located at $x = 50$ m in a pipe of length 100 m, and results are reported at the time $t = 1.0$ s. Reference solutions are calculated by the flux-limited Roe scheme of [17], using a grid of 20 000 cells.

6.3.1 Convergence Test for the WIMF Scheme

We use a convective CFL number of $C = 1$, or more precisely

$$\frac{\Delta x}{\Delta t} = 13 \text{ m/s} \approx \max_{j,n} |(v_g)_j^n|. \tag{139}$$

The results of the WIMF scheme are plotted in Figure 5 for various grid sizes.

We observe an overshoot in the volume fraction for the coarsest grids. Apart from this, the WIMF

Table 3: Zuber-Findlay shock 1. Convergence rates for the WIMF scheme.

n	cells	$\|\|E\|\|_n$	s_n
1	50	2.181	
2	100	1.352	0.6897
3	200	0.746	0.8578
4	400	0.338	1.1417
5	800	0.256	0.4041
6	3200	0.0812	0.8269
7	10000	0.0352	0.7325

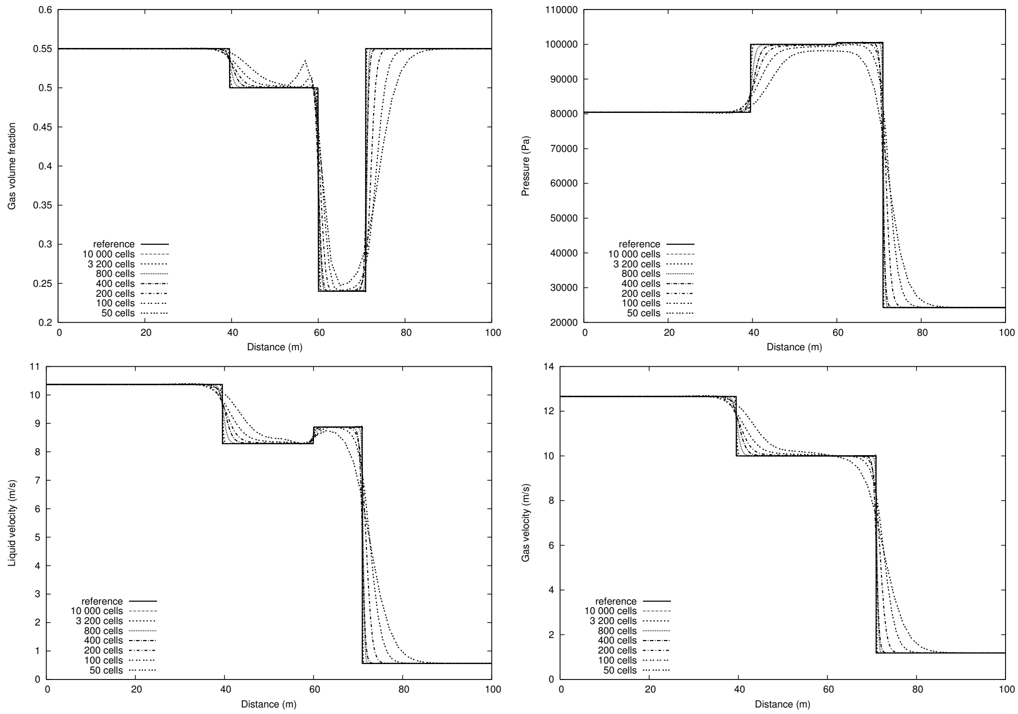

Figure 5: Zuber-Findlay shock tube 1. Grid refinement for the WIMF scheme. Top left: Gas volume fraction. Top right: Pressure. Bottom left: Gas velocity. Bottom right: Liquid velocity.

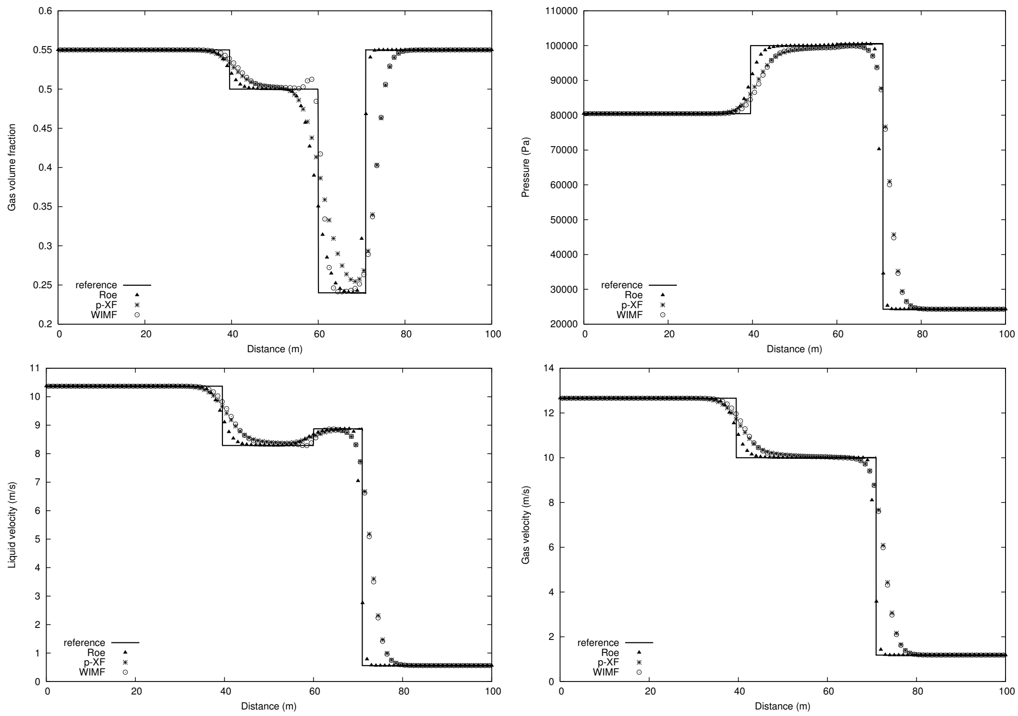

Figure 6: Zuber-Findlay shock tube 1. Roe, p-XF and WIMF schemes, 100 cells. Top left: Gas volume fraction. Top right: Pressure. Bottom left: Gas velocity. Bottom right: Liquid velocity.

scheme convergences smoothly to the reference solution. Convergence rates for the gas volume fraction are given in Table 3.

6.3.2 Comparison between the Various Schemes

In Figure 6, the results of WIMF and p-XF are compared with the first-order Roe scheme, for a grid of 100 cells. For the WIMF and p-XF schemes we used a convective CFL number of $C = 1$ as given by (139). For the Roe scheme, we used

$$\frac{\Delta x}{\Delta t} = 32.6 \text{ m/s}, \tag{140}$$

corresponding to the CFL criterion for the *sonic* waves, $C = 0.4$ with respect to convection.

We observe that the p-XF and WIMF schemes provide a similar resolution of the sonic waves, whereas they are both inferior to the Roe scheme in this respect. We further observe that WIMF gives a sharper resolution of the contact wave than Roe, but as previously noted, also introduces an overshoot.

6.4 Zuber-Findlay Shock 2

We now consider a second shock tube problem using the same Zuber-Findlay slip law (135)–(136) as in the previous example. This problem was investigated as Example 3 by Baudin et al. [1]. We here follow in their footsteps and modify the gas pressure law; in the context of (8), we use

$$a_{\mathrm{g}} = 300 \text{ m/s} \tag{141}$$

instead of

$$a_{\mathrm{g}} = \sqrt{10^5}\ \mathrm{m/s} \tag{142}$$

which is used for all other numerical examples of this paper. However, as for our other simulations, the liquid remains compressible as described by (7).

We also follow Baudin et al. [1] in transforming to the variables (see also Section 5.1):

ρ - mixture density,
Y - gas mass fraction,
v - mixture velocity.

Herein, v is expressed as

$$v = \frac{m_{\mathrm{g}} v_{\mathrm{g}} + m_\ell v_\ell}{\rho}. \tag{143}$$

In this formulation, the initial states are given by [1]

$$\mathbf{W}_{\mathrm{L}} = \begin{bmatrix} \rho \\ Y \\ v \end{bmatrix} = \begin{bmatrix} 453.197\ \mathrm{kg/m^3} \\ 0.00705 \\ 24.8074\ \mathrm{m/s} \end{bmatrix} \tag{144}$$

and

$$\mathbf{W}_{\mathrm{R}} = \begin{bmatrix} \rho \\ Y \\ v \end{bmatrix} = \begin{bmatrix} 454.915\ \mathrm{kg/m^3} \\ 0.0108 \\ 1.7461\ \mathrm{m/s} \end{bmatrix}. \tag{145}$$

The initial discontinuity is located at $x = 50$ m in a pipe of length 100 m, and results are reported at the time $t = 0.5$ s. The flux-limited Roe scheme on a grid of 20 000 cells was used to compute the reference solutions.

6.4.1 Convergence Test for the WIMF Scheme

We use a convective CFL number of 1, or more precisely

$$\frac{\Delta x}{\Delta t} = 30\ \mathrm{m/s}, \tag{146}$$

corresponding to the maximum gas velocity occurring during the simulation.

The results of the WIMF scheme are plotted in Figure 7 for various grid sizes. Convergence rates, with respect to the gas mass fraction Y, are given in Table 4. We observe that the WIMF scheme converges uniformly to the reference solution, and for this case no overshoots are visible.

Table 4: Zuber-Findlay shock 2. Convergence rates for the WIMF scheme.

n	cells	$\|\|E\|\|_n$	s_n
1	100	$7.204 \cdot 10^{-3}$	
2	200	$4.864 \cdot 10^{-3}$	0.5669
3	400	$3.208 \cdot 10^{-3}$	0.6005
4	800	$2.220 \cdot 10^{-3}$	0.5420
5	3200	$9.501 \cdot 10^{-4}$	0.6067
6	10000	$4.819 \cdot 10^{-4}$	0.5958

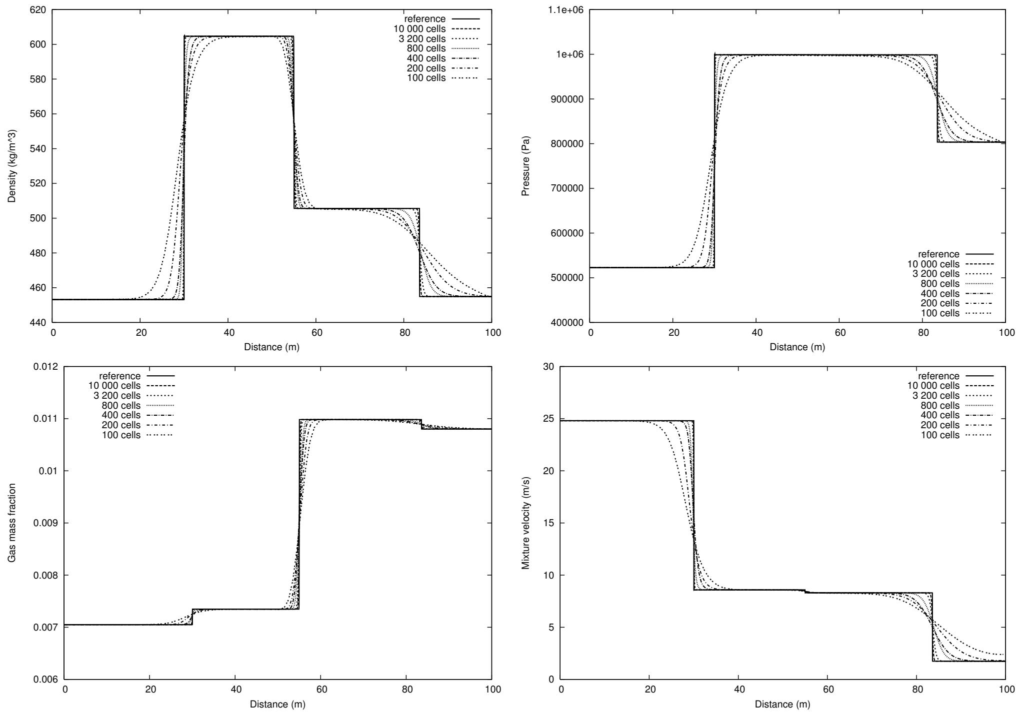

Figure 7: Zuber-Findlay shock 2. Grid refinement for the WIMF scheme. Top left: Mixture density. Top right: Pressure. Bottom left: Gas mass fraction. Bottom right: Density-averaged velocity.

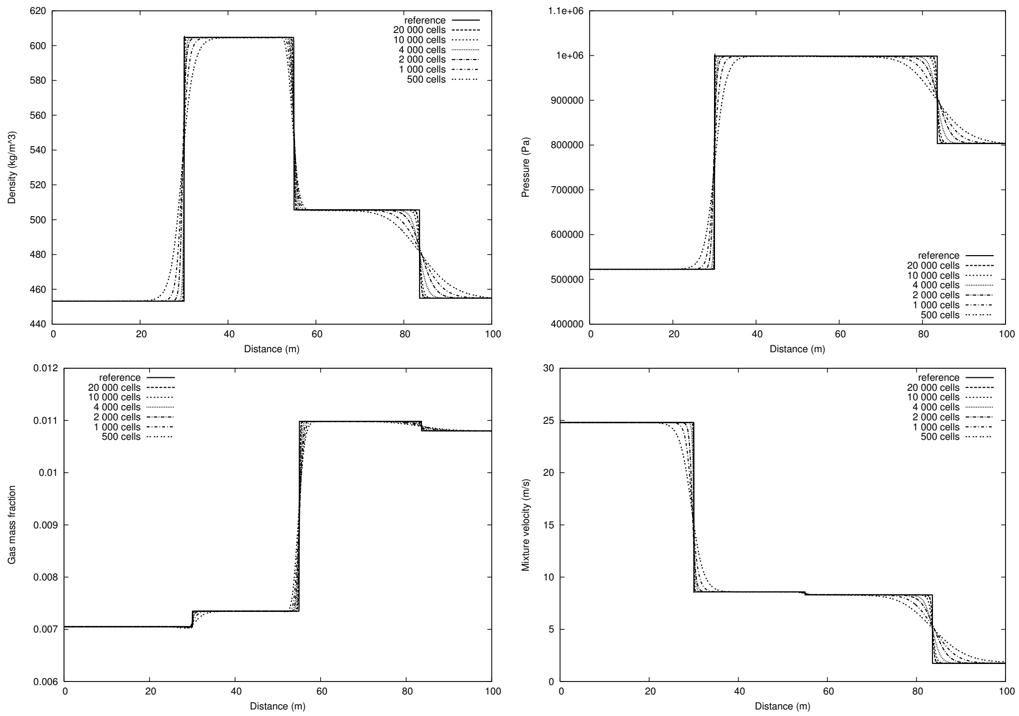

Figure 8: Zuber-Findlay shock 2. Grid refinement for the implicit p-XF scheme. Top left: Mixture density. Top right: Pressure. Bottom left: Gas mass fraction. Bottom right: Density-averaged velocity.

6.4.2 Convergence Test for the p-XF Scheme

We now use a time step 4 times larger than for the WIMF scheme, i.e. in the context of (122) we use $C = 4$. Hence the CFL condition (1) is violated with respect to all waves of the system.

The results of the p-XF scheme are plotted in Figure 8 for various grid sizes. We observe that also the p-XF scheme converges to the reference solution in a fully non-oscillatory manner. Due to the increased time step, there is a significant amount of numerical diffusion, enforcing the use of fine grids. However, as can be seen by Table 5, the convergence rate – with respect to gas mass fraction – is comparable to that of WIMF.

Remark 3. *This example illustrates that* p-XF *qualifies as a* **strongly implicit** *scheme whereas* WIMF *is* **weakly implicit** *by the terminology of [12].*

Table 5: Zuber-Findlay shock 2. Convergence rates for the p-XF scheme.

n	cells	$\|\|E\|\|_n$	s_n
1	500	$4.783 \cdot 10^{-3}$	
2	1000	$3.343 \cdot 10^{-3}$	0.5168
3	2000	$2.285 \cdot 10^{-3}$	0.5488
4	4000	$1.546 \cdot 10^{-3}$	0.5637
5	10000	$9.068 \cdot 10^{-4}$	0.5824
6	20000	$5.955 \cdot 10^{-4}$	0.6067

6.5 A More Complex Slip Relation

The purpose of this final test is to investigate the performance of the WIMF scheme for more realistic slip relations which do not have a simple linear form such as (10). In addition, this case features transitions between genuine two-phase and pure liquid regions. These are both challenges that are relevant for industrial applications of the drift-flux model.

6.5.1 The Test Case

This case was introduced as Example 4 by Evje and Fjelde [9], and has been further investigated by Munkejord et al. [17, 26]. We consider a pipe of total length $L = 1000$ m which is initially filled with almost-pure liquid ($\alpha_{\mathrm{g}} = 10^{-7}$). During the first 10 seconds of the simulation, the inlet liquid and gas mass flowrates are increased from zero to 12.0 kg/s and 0.08 kg/s respectively. The liquid flow rate is then kept constant for the rest of the simulation. At the time $t = 50$ s, the inlet gas mass flow rate is linearly decreased to zero in 20 s, and for the rest of the simulation only liquid flows into the pipe. Throughout the simulation, the outlet pressure is kept constant at 10^5 Pa. The results are reported at $t = 175$ s.

6.5.2 The Slip Relation

We use the same nonlinear slip law as the previous works [9, 17, 26]. Writing the law on the standard form (10), we take K to be constant, whereas S is allowed to depend on α_ℓ in a non-linear way. In particular, we use the parameters

$$K = 1.0 \qquad S = S(\alpha_\ell) = \sqrt{\alpha_\ell} \times 0.5 \text{ m/s}, \tag{147}$$

which may be viewed as a more complicated form of the dispersed slip law (126).

6.5.3 Friction Terms

For this test case, we follow Evje and Fjelde [9] and include a simple friction model. More precisely, in the context of (4) we choose

$$Q = -\frac{32 v_{\mathrm{mix}} \mu_{\mathrm{mix}}}{d^2}. \tag{148}$$

Here $d = 0.1$ m is the diameter of the pipe. Furthermore, v_{mix} is the mixture velocity

$$v_{\mathrm{mix}} = \alpha_{\mathrm{g}} v_{\mathrm{g}} + \alpha_\ell v_\ell \tag{149}$$

and μ_{mix} is the mixture viscosity

$$\mu_{\mathrm{mix}} = \alpha_{\mathrm{g}} \mu_{\mathrm{g}} + \alpha_\ell \mu_\ell. \tag{150}$$

Here

$$\mu_{\mathrm{g}} = 5 \times 10^{-6} \text{ Pa} \cdot \text{s} \qquad \text{and} \qquad \mu_\ell = 5 \times 10^{-2} \text{ Pa} \cdot \text{s}. \tag{151}$$

6.5.4 Discretization of the Friction Terms

For the Roe scheme, we used an explicit forward Euler discretization of the source terms. For the WIMF scheme, we have discretized (148) as

$$\widetilde{Q}_j = -\frac{32}{d^2} (\mu_{\mathrm{mix}})_j^n \, (\widetilde{v_{\mathrm{mix}}})_j \,, \tag{152}$$

where $(\widetilde{v_{\text{mix}}})_j$ is calculated in a linearly implicit manner as

$$(\widetilde{v_{\text{mix}}})_j = \frac{(\widetilde{\rho_g \alpha_g v_g})_j}{(\rho_g)_j^n} + \frac{(\widetilde{\rho_\ell \alpha_\ell v_\ell})_j}{(\rho_\ell)_j^n}. \tag{153}$$

Using this, we discretize the right hand sides of (106) and (107) as

$$\left(\frac{\widetilde{m_k}}{\rho} Q\right)_j = \left(\frac{m_k}{\rho}\right)_j^n \widetilde{Q}_j. \tag{154}$$

In this manner, the scheme retains its linearity in the implicit terms.

6.5.5 Performance of the Roe and WIMF Schemes

For the WIMF scheme, we used the time step

$$\frac{\Delta x}{\Delta t} = 3.8 \text{ m/s}, \tag{155}$$

corresponding to a convective CFL number $C = 1$ as given by (122). For the Roe scheme, we used a CFL number $C = 0.9$ with respect to *sonic* propagation, which for this case is approximately

$$a_l = 1000 \text{ m/s} \tag{156}$$

due to the single-phase liquid regions.

It is worth emphasizing that implicit methods are particularly useful on cases involving such single-phase liquid regions, due to the strict CFL requirements imposed by the rapid sonic propagation. Here

$$\Delta t^{\text{WIMF}} / \Delta t^{\text{Roe}} \approx 300, \tag{157}$$

and the efficiency differences between the Roe and WIMF schemes are *significant*.

6.5.6 Comparison between the Roe and WIMF Schemes

Results for the first-order Roe and WIMF schemes are given in Figure 9, with a grid of 200 cells. The reference solution was computed by the flux-limited Roe scheme, using a grid of 10 000 cells and CFL number $C = 0.5$.

Note that the highly improved efficiency of the WIMF scheme is accompanied by a similar improvement in the resolution of the slow dynamics, as was also seen in Sections 6.1 and 6.3. This attractive behaviour was also observed in [11, 12] for the two-fluid version of WIMF.

Table 6: Mass transport problem, WIMF scheme. Convergence rates with respect to volume fraction.

n	cells	$\|\|E\|\|_n$	s_n
1	200	16.442	
2	400	9.642	0.7699
3	800	5.982	0.6889
4	4000	1.557	0.8363

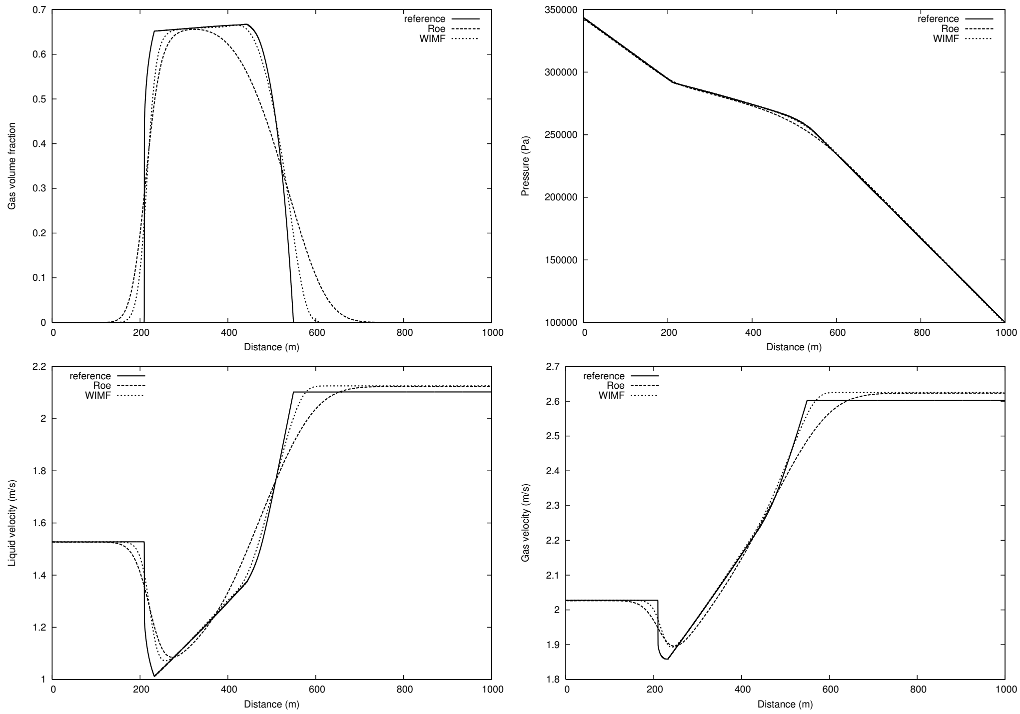

Figure 9: Mass transport problem. WIMF vs Roe scheme, 200 cells. Top left: Gas volume fraction. Top right: Pressure. Bottom left: Liquid velocity. Bottom right: Gas velocity.

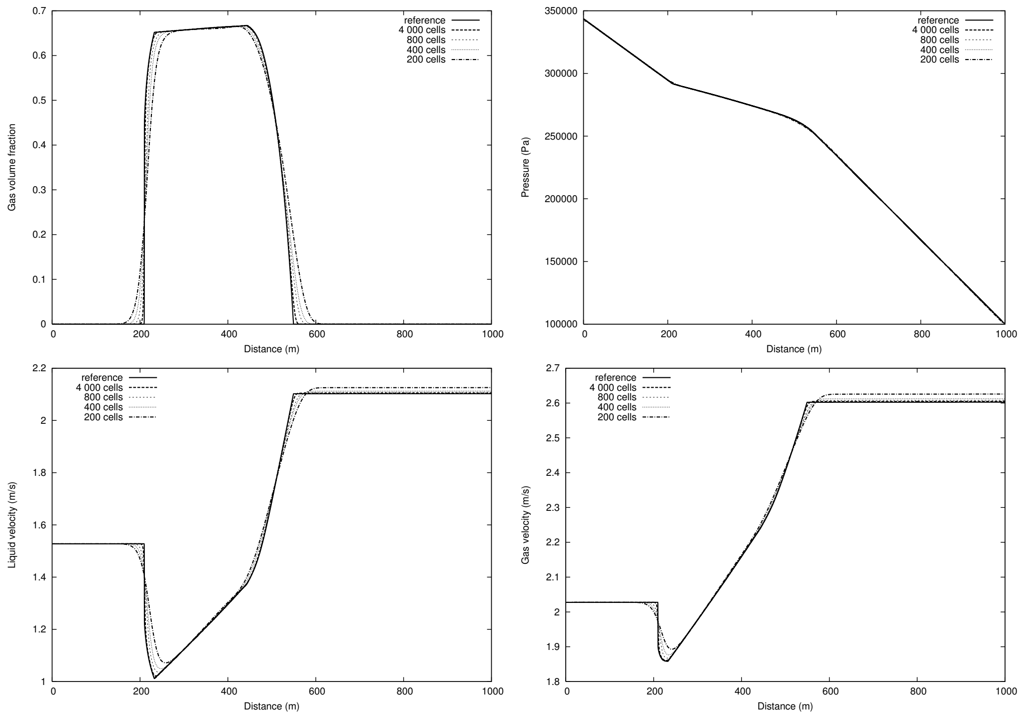

Figure 10: Mass transport problem. Convergence of the WIMF scheme, convective CFL number $C = 1$. Top left: Gas volume fraction. Top right: Pressure. Bottom left: Liquid velocity. Bottom right: Gas velocity.

6.5.7 Convergence

As seen by Figure 10 and Table 6, the WIMF scheme converges to the same solution as the Roe scheme as the grid is refined. This is reassuring in light of the large disparity of the time steps, as well as the inclusion of boundary conditions and source terms.

It should however be noted that for grids of less than 200 cells, the WIMF scheme requires a somewhat lower CFL number for stability.

7 Conclusion

We have presented an implicit pressure-based central type scheme for a drift-flux two-phase model, denoted as p-XF. Generalizing a technique introduced in [11], denoted as WIMF, we have incorporated explicit upwind-type fluxes allowing for an accurate resolution of the mass transport waves of the system. The WIMF scheme improves on the accuracy of p-XF with little loss of stability, and is the scheme we propose for practical applications.

A difficulty with the drift-flux model is that its formulation is sensitive to the specification of the closure law Φ, which may vary depending on the flow conditions of the application.

In this paper, the numerical schemes have been derived by basing the implicit approximation of the fluxes on a linearization around the slip $\Phi = 0$. By this, we ensure certain accuracy and robustness properties for this particular case.

The numerical examples demonstrate that the desirable properties of the schemes essentially carry over to more general choices of Φ. The schemes are conservative in all numerical fluxes and consistent with a given slip relation, and numerical evidence confirms that convergence to correct solutions are obtained.

Numerical overshoots and oscillations in some cases occur for the mass transport wave. We observe that such oscillations may to a large extent be tamed by reducing the CFL number.

The WIMF scheme outperforms the explicit Roe scheme in terms of efficiency and accuracy on slow dynamics, and results compare well to existing semi-implicit methods presented in the literature [2, 15]. This demonstrates that the WIMF strategy introduced in [11] has applicability beyond the two-fluid model originally considered.

With this paper, we have presented a general setting for the construction of WIMF type schemes and by that hope to pave the way for further application to additional models. In particular, the WIMF approach seems useful for models where the eigenstructure is too complicated for an efficient construction of approximate Riemann solvers.

Acknowledgements

The authors thank the Research Council of Norway for financial support.

References

[1] M. Baudin, C. Berthon, F. Coquel, R. Masson and Q. H. Tran, A relaxation method for two-phase flow models with hydrodynamic closure law, *Numer. Math.* **99**, 411–440, 2005.

[2] M. Baudin, F. Coquel and Q. H. Tran, A semi-implicit relaxation scheme for modeling two-phase flow in a pipeline, *SIAM J. Sci. Comput.* **27**, 914–936, 2005.

[3] K. H. Bendiksen, An experimental investigation of the motion of long bubbles in inclined tubes, *Int. J. Multiphase Flow* **10**, 467–483, 1984.

[4] K. H. Bendiksen, D. Malnes, R. Moe and S. Nuland, The dynamic two-fluid model OLGA: Theory and application, *SPE Prod. Eng.* **6**, 171–180, (1991).

[5] J. A. Bouré, Wave phenomena and one-dimensional two-phase flow models, *Multiphase Sci. Tech.* **9**, 1-107, 1997.

[6] J. Cortes, A. Debussche and I. Toumi, A density perturbation method to study the eigenstructure of two-phase flow equation systems, *J. Comput. Phys.* **147**, 463–484, 1998.

[7] W. Dai and P. R. Woodward, A high-order iterative implicit-explicit hybrid scheme for magnetohydrodynamics, *SIAM J. Sci. Comput* **19**, 1827–1846, 1998.

[8] S. Evje and K. K. Fjelde, Hybrid flux-splitting schemes for a two-phase flow model. *J. Comput. Phys.* **175**, 674–701, 2002.

[9] S. Evje and K. K. Fjelde, On a rough AUSM scheme for a one-dimensional two-phase model, *Comput. Fluids* **32**, 1497–1530, 2003.

[10] S. Evje and T. Flåtten, Hybrid central-upwind schemes for numerical resolution of two-phase flows, *ESAIM-Math. Model. Num.* **39**, 253–274, 2005.

[11] S. Evje and T. Flåtten, Weakly implicit numerical schemes for a two-fluid model, *SIAM J. Sci. Comput.* **26**, 1449–1484, 2005.

[12] S. Evje and T. Flåtten, CFL-violating numerical schemes for a two-fluid model, *J. Sci. Comput.* **29**, 83–114, 2006.

[13] S. Evje and T. Flåtten, On the wave structure of two-phase flow models, *SIAM J. Appl. Math.* **67**, 487–511, 2007.

[14] S. Evje, T. Flåtten and H. A. Friis, On a relation between pressure-based schemes and central schemes for hyperbolic conservation laws, *Numer. Meth. Part. Diff. Eq.* **24**, 605–645, 2008.

[15] I. Faille and E. Heintzé, A rough finite volume scheme for modeling two-phase flow in a pipeline, *Comput. Fluids* **28**, 213–241, 1999.

[16] K. Falk, *Pressure pulse propagation in gas-liquid pipe flow*, Dr. Ing. thesis, Department of Petroleum Engineering, NTNU, Norway, 1999.

[17] T. Flåtten and S. T. Munkejord, The approximate Riemann solver of Roe applied to a drift-flux two-phase flow model, *ESAIM-Math. Model. Num.* **40**, 735–764, 2006.

[18] F. França and R. T. Lahey, Jr, The use of drift-flux techniques for the analysis of horizontal two-phase flows, *Int. J. Multiphase Flow* **18**, 787–801, 1992.

[19] S. L. Gavrilyuk and J. Fabre, Lagrangian coordinates for a drift-flux model of a gas–liquid mixture, *Int. J. Multiphase Flow* **22**, 453–460, 1996.

[20] A. Harten and P. D. Lax, On a class of high resolution total-variation-stable finite-difference schemes, *SIAM J. Numer. Anal.* **21**, 1–23, 1984.

[21] T. Hibiki and M. Ishii, Distribution parameter and drift velocity of drift-flux model in bubbly flow, *Int. J. Heat Mass Tran.* **45**, 707–721, 2002.

[22] T. Y. Hou and P. G. Le Floch, Why nonconservative schemes converge to wrong solutions: error analysis, *Math. Comput.* **62**, 497–530, 1994.

[23] M. Larsen, E. Hustvedt, P. Hedne, and T. Straume, Petra: A novel computer code for simulation of slug flow, in *SPE Annual Technical Conference and Exhibition*, Society of Petroleum Engineers, 1997.

[24] R. J. Lorentzen and K. K. Fjelde, Use of slopelimiter techniques in traditional numerical methods for multi-phase flow in pipelines and wells, *Int. J. Numer. Meth. Fluids* **48**, 723–745, 2005.

[25] J. M. Masella, Q. H. Tran, D. Ferre and C. Pauchon, Transient simulation of two-phase flows in pipes, *Int. J. Multiphase Flow* **24**, 739–755, 1998.

[26] S. T. Munkejord, S. Evje and T. Flåtten, The multi-stage centred-scheme approach applied to a drift-flux two-phase flow model, *Int. J. Numer. Meth. Fluids* **52**, 679–705, 2006.

[27] S. V. Patankar, *Numerical Heat Transfer and Fluid Flow*, Taylor & Francis, Philadelphia, 1980.

[28] C. Pauchon, H. Dhulesia, D. Lopez and J. Fabre, TACITE: A Comprehensive Mechanistic Model for Two-Phase Flow, *BHRG Conference on Multiphase Production*, Cannes, June 1993.

[29] A. Prosperetti and G. Tryggvason (Editors), Computational Methods for Multiphase Flow, *Cambridge University Press, New York*, 2007.

[30] V. H. Ransom and D. L. Hicks. Hyperbolic two-pressure models for two-phase flow, *J. Comput. Phys.* **53**, 124–151, 1984.

[31] J. E. Romate, An approximate Riemann solver for a two-phase flow model with numerically given slip relation, *Comput. Fluids* **27**, 455–477, 1998.

[32] H. B. Stewart and B. Wendroff, Review article; two-phase flow : Models and methods, *J. Comput. Phys.* **56**, 363–409, 1984.

[33] E. Tadmor, Numerical viscosity and the entropy condition for conservative difference schemes, *Math. Comput.* **43**, 369–381, 1984.

[34] E. F. Toro, *Riemann solvers and numerical methods for fluid dynamics*, 2nd Ed., Springer-Verlag, Berlin, 1999.

[35] I. Toumi and D. Caruge, An Implicit Second-Order Numerical Method for Three-Dimensional Two-Phase Flow Calculations, *Nucl. Sci. Eng.* **130**, 213–225, 1998.

[36] N. Zuber and J. A. Findlay, Average volumetric concentration in two-phase flow systems, *J. Heat Transfer* **87**, 453–468, 1965.